

Soil carbon dioxide flux partitioning in a calcareous watershed with agricultural impacts

Caitlin Hodges¹, Susan L. Brantley¹, Melika Sharifronizi¹, Brandon Forsythe¹, Qicheng Tang¹, Nathan Carpenter¹, and Jason Kaye¹

¹Pennsylvania State University

November 22, 2022

Abstract

Predicting the partitioning between aqueous and gaseous C across landscapes is difficult because many factors interact to control CO₂ concentrations and removal as DIC. For example, carbonate minerals may buffer soil pH so that CO₂ dissolves in porewaters, but nitrification of fertilizers may decrease pH so that carbonate weathering results in a gaseous CO₂ efflux. Here, we investigate CO₂ production and dissolution in an agricultural, first-order, mixed-lithology humid, temperate watershed. We quantified soil mineralogy and measured porewater chemistry, soil moisture, and pCO₂ and pO₂ as a function of depth at three hillslope positions for a year. The variation of soil moisture along the hillslope was the dominant control on the concentration of soil CO₂, but mineralogy acted as a secondary control on the partitioning of CO₂ between the gaseous and aqueous phases. The regression slopes of pCO₂ vs. pO₂ in the carbonate-bearing soils indicate a deficit of CO₂ relative to O₂ ($p < 0.05$). Additionally, we found no abiotic gaseous CO₂ efflux from carbonate weathering. We concluded that in the calcareous soils, about a third of respired C dissolves and drains from the soil rather than diffusing out to the atmosphere. To represent the global scope of the reactions we evaluated at our local watershed, we used databases of carbonate minerals and land uses to map types of soil degassing behaviors. Based on our maps, the partitioning of respired soil CO₂ to the aqueous phase may be globally common and should be accounted for in ecosystem C budgets and models.

Hosted file

hodes colefarm supplemental file for submission jgrb.docx available at <https://authorea.com/users/353533/articles/598526-soil-carbon-dioxide-flux-partitioning-in-a-calcareous-watershed-with-agricultural-impacts>

Hosted file

essoar.10506704.1.docx available at <https://authorea.com/users/353533/articles/598526-soil-carbon-dioxide-flux-partitioning-in-a-calcareous-watershed-with-agricultural-impacts>

1
2
3
4

Soil carbon dioxide flux partitioning in a calcareous watershed with agricultural impacts

5 **Caitlin Hodges^{1*}, Susan L. Brantley^{2,3}, Melika Sharifironizi², Brandon Forsythe², Qicheng**
6 **Tang¹, Nathan Carpenter³, Jason Kaye¹**

7 ¹Pennsylvania State University, Department of Ecosystem Science and Management, University
8 Park, PA

9 ²Pennsylvania State University, Earth and Environmental Systems Institute, University Park, PA

10 ³Pennsylvania State University, Department of Geosciences, University Park, PA

11

12 Corresponding author: Caitlin Hodges (cah423@psu.edu)

13

Key Points:

- 15 • Carbonate mineralogy increases the dissolved inorganic carbon flux out of soils in an
16 agricultural, humid temperate watershed
- 17 • This flux of dissolved inorganic carbon represents 43% of all respired carbon dioxide in
18 the soil containing the most carbonates
- 19 • Surface carbon dioxide efflux measurements would substantially underestimate soil
20 respiration rates in this watershed
21

22 Abstract

23 Predicting the partitioning between aqueous and gaseous C across landscapes is difficult
24 because many factors interact to control CO₂ concentrations and removal as DIC. For example,
25 carbonate minerals may buffer soil pH so that CO₂ dissolves in porewaters, but nitrification of
26 fertilizers may decrease pH so that carbonate weathering results in a gaseous CO₂ efflux. Here,
27 we investigate CO₂ production and dissolution in an agricultural, first-order, mixed-lithology
28 humid, temperate watershed. We quantified soil mineralogy and measured porewater chemistry,
29 soil moisture, and pCO₂ and pO₂ as a function of depth at three hillslope positions for a year. The
30 variation of soil moisture along the hillslope was the dominant control on the concentration of
31 soil CO₂, but mineralogy acted as a secondary control on the partitioning of CO₂ between the
32 gaseous and aqueous phases. The regression slopes of pCO₂ vs. pO₂ in the carbonate-bearing
33 soils indicate a deficit of CO₂ relative to O₂ ($p < 0.05$). Additionally, we found no abiotic gaseous
34 CO₂ efflux from carbonate weathering. We concluded that in the calcareous soils, about a third
35 of respired C dissolves and drains from the soil rather than diffusing out to the atmosphere. To
36 represent the global scope of the reactions we evaluated at our local watershed, we used
37 databases of carbonate minerals and land uses to map types of soil degassing behaviors. Based
38 on our maps, the partitioning of respired soil CO₂ to the aqueous phase may be globally common
39 and should be accounted for in ecosystem C budgets and models.

40

41 Plain Language Summary

42 Carbon dioxide (CO₂) produced by roots and microbes in soil is a key component of the global
43 carbon cycle. Generally, respired CO₂ exits soil as a gas. However, CO₂ also dissolves in soil
44 porewaters during weathering reactions in soils, especially with carbonate minerals. These
45 reactions reduce the amount of CO₂ exiting the soil surface. Conversely, agricultural production

46 may create conditions that drive CO₂ in carbonates into the gas phase. These reactions in
47 agricultural soils may increase the amount of CO₂ leaving the soil surface. We investigated when
48 these reactions may be important in decreasing or increasing the amount of CO₂ exiting the soil
49 surface. In soils containing carbonate minerals, we found that respired CO₂ drove weathering of
50 carbonate minerals and thus decreased the amount of CO₂ that exits the soil surface by one third.
51 We found no evidence of agricultural land use generating conditions that drive CO₂ from
52 carbonate minerals into the gas phase. Our results indicate that measurements of soil surface CO₂
53 flux measurements would underestimate the amount of CO₂ produced by plant roots and
54 microbes. These reactions are common in soils and should be accounted for in global C cycle
55 models.

56

57 **1 Introduction**

58 Soil respiration represents a key component of the global carbon (C) cycle, as it is the
59 largest flux of C from terrestrial systems over annual timescales (Amundson, 2001). In many
60 cases, the flux of CO₂ from the soil surface equals the CO₂ produced by respiring roots and
61 organisms in soil (Cerling, 1984). Indeed, most ecosystem carbon cycle models, from plot to
62 global scale, simulate soil CO₂ flux as equivalent to soil respiration (Oleson et al., 2010; Shi et
63 al., 2018; Thornton et al., 2002). Soil C flux (soil respiration) is most often simulated as a
64 function of soil temperature and moisture (Brook et al., 1983; Lloyd & Taylor, 1994; Raich &
65 Schlesinger, 1992). However, respired CO₂ has the potential to participate in a range of reactions
66 in the soil system that may lower the measured soil CO₂ flux by over 50% (Chadwick et al.,
67 1994; Hamerlynck et al., 2013; Hodges et al., 2019; Olshansky et al., 2019; Rey, 2015; Sánchez-
68 Cañete et al., 2018). Indeed, researchers with interest in long-term C cycling emphasize
69 sequestration of C as alkalinity in soil pore fluids during weathering over geological time periods

70 (Brantley et al., 2014). Incorporating these reactions into modern-day ecosystem models could
71 improve C cycle projections.

72 Reactions of water and minerals with CO₂ in the soil system are not included in our
73 ecosystem models at least partly because the extent and magnitude of each reaction is unclear,
74 especially for soils formed at different landscape positions or with different mineralogy. For
75 example, Olshansky et al. (2019) report that drainage of soil waters through a midslope soil
76 reduced total CO₂ efflux by two thirds due to dissolution of gaseous CO₂ and removal
77 downslope. Similarly, in calcareous soils, increasing soil water content enhances carbonate
78 dissolution and serves to increase partitioning of inorganic carbon to the aqueous phase (Kim et
79 al., 2020; Mikhailova & Post, 2006; Wu et al., 2008). However, abiotic reactions may also be a
80 source of CO₂ with respect to the soil atmosphere. For example, land management associated
81 with agricultural production can lower soil pH so that weathering of carbonate minerals becomes
82 a source of abiotic CO₂ to the soil atmosphere, augmenting soil CO₂ flux (Sanderman, 2012;
83 West & McBride, 2005; Zamanian et al., 2018). The magnitude of this potential abiotic gaseous
84 CO₂ flux is controlled by soil buffering capacity and nitrification rate (Hamilton et al., 2007).
85 Therefore, our goal was to determine the role of landscape position and mineralogy in the
86 production of CO₂ and the subsequent partitioning of that soil CO₂ between the aqueous and
87 gaseous phase in a humid, temperate watershed affected by agricultural land-use. We then apply
88 our findings to refine predictions of where abiotic reactions with respired CO₂ may impact
89 measurements or models of soil respiration.

90 Our research site, the Susquehanna Shale Hills Critical Zone Observatory (SSHCZO), is
91 particularly well suited to this work because it includes contrasting lithologies of distinct
92 mineralogy and potential agricultural impacts. We hypothesized 1) that differences in soil

93 moisture by hillslope position would act as first-order controls on soil pCO₂ with wet hillslope
94 positions having higher pCO₂ than dryer positions due to well documented impacts of soil
95 moisture on respiration and diffusion (Brook et al., 1983; Hasenmueller et al., 2015). In this case,
96 soil pO₂ and pCO₂ is expected to follow a 1:1 molar relationship with respect to consumption of
97 O₂ and production of CO₂ following the stoichiometry of aerobic respiration corrected for
98 diffusion. However, we expected that this moisture-driven respiration-diffusion pattern could be
99 affected by mineralogy and nitrification. Specifically, we hypothesized 2) that in soils with more
100 carbonates, the carbonates would buffer soil pH so that some respired CO₂ would be partitioned
101 into the aqueous phase and exported in draining water such that the pCO₂ to pO₂ ratio of the soil
102 atmosphere would be lower than predicted. We additionally hypothesized 3) that this dissolved
103 CO₂ in draining soil waters would represent removal of the respired CO₂ from the soil. This
104 would contrast with our results from the nearby Shale Hills watershed where CO₂ dissolution and
105 subsequent mineral weathering had no significant effect on soil CO₂ efflux on annual timescales
106 (Hasenmueller et al., 2015; Hodges et al., 2019; Jin et al., 2014).

107 For agriculturally impacted soils, we hypothesized 4) that nitrate-associated acidity in
108 porewaters accelerates carbonate mineral dissolution and drives abiotic, mineral-derived CO₂
109 into the gaseous phase. This tests the predictions that nitrification-associated acidity drives
110 carbonate-derived CO₂ into the gas phase (Zamanian et al., 2018, 2021), since acidity produced
111 during nitrification favors lower pH values and therefore, gaseous, rather than dissolved, CO₂.

112 If hypotheses 2 and 3 are supported, then measurements of soil CO₂ efflux at our field
113 site likely underestimate soil respiration. If hypothesis 4 is supported, then soil CO₂ efflux at our
114 site likely represents a combination of respiration and abiotically generated CO₂. Either of these

115 results would represent a significant departure from the standard assumption that soil CO₂ efflux
116 equals soil respiration.

117 To test our hypotheses, we monitored soil pCO₂, pO₂, moisture, temperature, and solution
118 chemistry in soils at three hillslope positions over a growing season in a cultivated landscape
119 developed on carbonate- and silicate-containing lithologies. We then linked the differences in
120 patterns of the soil gases and solution chemistry to moisture and mineralogical differences at
121 each hillslope position. Finally, by considering results at the SSHCZO, we used the World
122 Inventory of Soil Emission Potentials and Global Food Security and Support databases to
123 identify the soils and regions where the presence of carbonate minerals impacts soil pCO₂
124 partitioning between gas and aqueous phases, causing CO₂ flux measurements to be poor
125 predictors of soil respiration.

126 **2 Materials and Methods**

127 **2.1 Site Description**

128 Measurements were focused in the Cole Farm watershed of the SSHCZO. The SSHCZO is in the
129 Ridge and Valley physiographic province of central Pennsylvania, USA, which is characterized
130 by folded and sometimes steeply dipping sedimentary rock. The Cole Farm catchment of the
131 SSHCZO is a small (0.65 km²) watershed underlain by calcareous shales of the Wills Creek and
132 Bloomsburg-Mifflintown formations containing interbedded shaley limestone, dolomite,
133 sandstone, and siltstone (Fig. 1; see supplement for mineralogy of local lithologies).

134 This site has been in active agricultural production since the early 1800s (Li et al., 2018).
135 Recent work in the watershed indicates limited sediment erosion from European settlement and
136 agricultural production (Silverhart, 2019). The three hillslope positions are not under agricultural
137 management, but the two midslope soils are downslope of fields in active production. Specific

138 fertilizer application rates to the agricultural fields upslope of the midslopes are unknown for the
 139 2018 growing season, but urea, $(\text{NH}_4)_2\text{SO}_4$, $(\text{NH}_4)_2\text{HPO}_4$, and potash were applied to the fields in
 140 addition to cow manure.

141 Within the catchment, four sites were chosen for soil characterization and long-term
 142 monitoring on the east midslope, west midslope, ridgetop, and valley floor. Monitoring of the
 143 valley floor site was abandoned due to consistent flooding throughout the growing season. The
 144 ridgetop site, CFRT, is located within the Bloomsburg-Mifflintown Formation that remains as a
 145 small forested ridge above the cultivated fields. Both midslope sites are downhill of the ridge on
 146 Wills Creek Formation. CFRT lies at the head of a swale and the two midslope sites are located

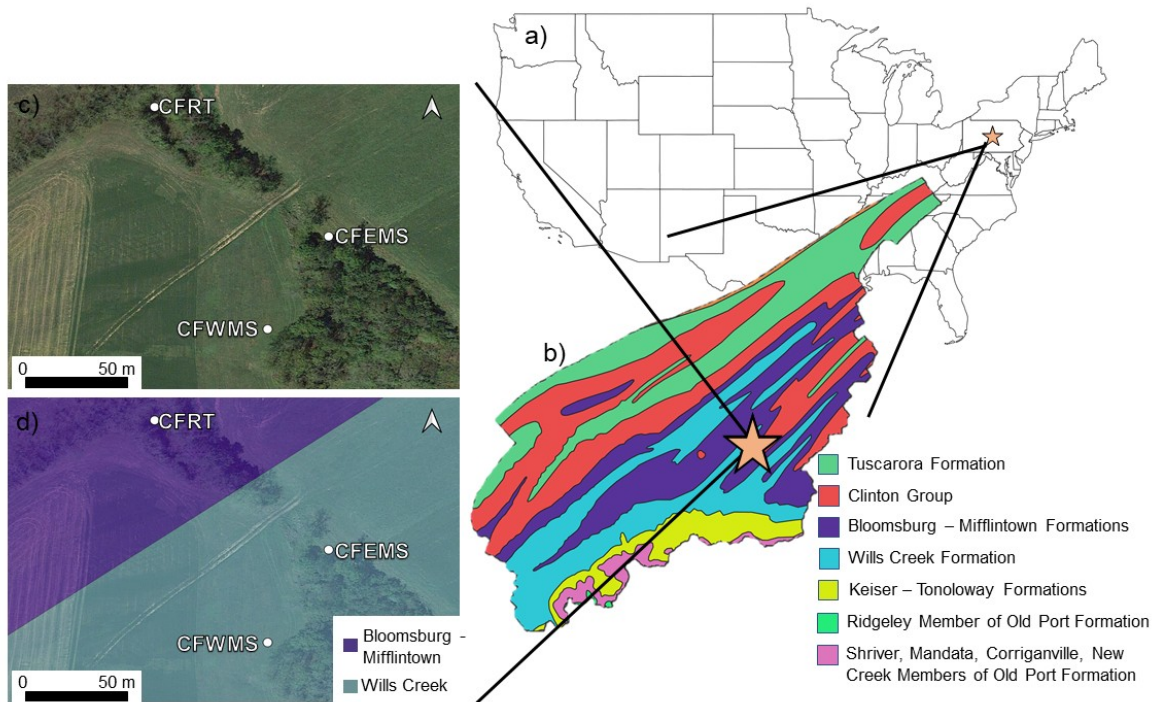


Fig 1: The Cole Farm watershed in the context of the United States (a), the broader Shavers Creek watershed (b), and zoomed-in to indicate vegetation and long-term sampling locations (c), and underlying bedrock formations (d).

147 along the swale which runs between an eastern and western cultivated field (Fig. 1). The swale
 148 collects runoff and groundwater from the surrounding agricultural production.

149

150 2.2 Soil Collection and Geochemical Analysis

151 Soil pits were dug at the east midslope (CFEMS), west midslope (CFWMS), ridgetop (CFRT)
152 locations (Fig. 1). Full soil pit descriptions for each site are published in the supplementary
153 materials of Li et al. (2018). The soils of Cole Farm are characterized by deep, fine particle size
154 class Alfisols. The two midslope soils, developed from calcareous shale of the Wills Creek
155 Formation, show little carbonate mineral content in the upper horizons, and a large increase in
156 carbonates at the C horizon. This is interpreted as evidence for almost complete carbonate
157 mineral dissolution in the upper horizons (see, for example, Figure 2), given that most of the
158 unweathered rock units reported in this Formation contain carbonate minerals (see appendix for
159 geochemical analysis of local bedrock). Furthermore, nearby soils similarly show such carbonate
160 depletion at the surface at a site with many sampling locations and wells (Brantley et al., 2013;
161 Gu et al., 2020). The ridgetop soil profile, developed from the Bloomsburg-Mifflintown
162 Formation, shows no evidence of higher carbonate abundance at depth most likely because the
163 parent lithology is not as calcareous as the Wills Creek.

164 Soils were sampled in 10 cm increments to bedrock (where bedrock was defined as the
165 limit of digging by backhoe). Bulk samples of the 10 cm increments representative of distinct
166 horizons were ground and digested using Li metaborate fusion for total elemental analysis.
167 Elemental analysis was performed on fusion digestates on a Perkin-Elmer Optima 5300,
168 Inductively Coupled Plasma Emission Spectrometer (ICP-AES, PerkinElmer, Waltham, MA,
169 USA). The bulk C-horizon samples were also ground to a fine powder and analyzed using X-Ray
170 diffraction with a Malvern Panalytical Empyrean X-Ray Diffractometer (Malvern Panalytical,
171 Malvern, Worcestershire, UK). Results from XRD were interpreted semi-quantitatively using

172 JADE software (International Centre for Diffraction Data, Newtown Square, PA, USA). Total
173 carbon of the bulk soils was analyzed on a CHNS-O elemental analyzer (Elemental Analyzer EA
174 1110, Thermo Fisher Scientific, Waltham, MA, USA).

175 2.3 Soil Gas Collection and Analysis

176 Soil gas samplers identical to those described in Hasenmueller et al. (2015) were installed in
177 triplicate at depths of interest at the three hillslope positions chosen to study soil gases. At
178 CFEMS and CFWMS soil pits, the gas samplers were installed at 20 cm and 40 cm depths, and
179 at a depth of 20 cm above the Cr horizon, which came to 108 cm in CFEMS and 190 cm in
180 CFWMS. At CFRT soil gas samplers were installed at 20 cm, 40 cm, 90 cm and 160 cm. All
181 statistical analyses were performed with only the data from the 20 and 40 cm gas wells, as the
182 deep wells were often filled with water at the CFEMS and CFWMS sites. Full pCO₂ and pO₂
183 datasets are published as corresponding data with this publication in Pangaea.

184 Soil gas tubes were sampled for pCO₂ and pO₂ (vol/vol %) every 3 wks from April 2018
185 through November 2018. Air-tight syringes with a one-way lock were used to sample the gas
186 tubes for pCO₂. All gas tubes were purged of 5 mL of gas in the 20 and 40 cm samplers, and 10
187 mL of gas in all samplers deeper than 40 cm to ensure sampling of soil atmosphere, and not dead
188 air in the sampling tube. Then 5 mL of soil gas was collected with the locking syringe for
189 analysis in the laboratory. Afterward, 10 mL of soil gas was sampled for pO₂ using a handheld
190 soil gas analyzer (model 901, Quantek Instruments). The Quantek 901 has a range of 0 to 100%
191 O₂ and an accuracy of ± 0.1 O₂. The Quantek was calibrated using O₂-free gas and ambient air.
192 Three samples of ambient air were collected with locking syringes 30 cm above the ground
193 surface per hillslope position for ambient CO₂. Soil gas samples were analyzed in the laboratory

194 on a flow-through infrared gas analyzer (LI-7000, LiCOR Inc.) within two days of collection.
195 Measurement accuracy is within 1% of measured value.

196 Soil pCO₂ and pO₂ samples were assessed based on the principles of apparent respiratory
197 quotient (ARQ) detailed in Angert et al. (2015) and are presented in this paper as outlined by
198 Hodges et al. (2019). Briefly, the soil gas data are plotted as pCO₂ vs. pO₂, relative to a line
199 defined by a slope of -0.76 and an x-axis origin of 20.95% (the concentration of O₂ in the
200 atmosphere). The line thus represents the 1:1 stoichiometry of the reaction describing oxidation
201 of generic organic matter (CH₂O) by O₂ and CO₂ production during cellular respiration (Eq. 1)
202 corrected for the ratio of the diffusion coefficients of CO₂ and O₂ in air (0.76).



204 Thus, if aerobic respiration and diffusion are the main controls on CO₂ and O₂
205 concentrations in soil then field data should plot relatively tightly near this theoretical line. In
206 contrast, significant deviations from this slope indicate that processes other than aerobic
207 respiration and gas diffusion control the soil pCO₂ or pO₂. The slope of the regression line is then
208 considered to show the predominant reaction defining the ARQ by dividing it by -0.76. An ARQ
209 of ~ 1 represents aerobic respiration (and gas diffusion). Anything above 1 indicates additional
210 CO₂ in the soil atmosphere compared to O₂, predicted based on the stoichiometry of aerobic
211 respiration. An ARQ below 1 indicates either less CO₂ relative to O₂, or less O₂ relative to CO₂
212 than predicted by the reaction stoichiometry (Angert et al., 2015).

213

214 2.4 Soil Porewater Collection and Analysis

215 Two porous cup tension lysimeters (Soil water samplers, 1900 and 1920 series, Soilmoisture
216 Equipment Corp., Santa Barbara, CA, USA) were installed at CFEMS, CFWMS, and CFRT in

217 June of 2017. The lysimeters were installed in hand-augered holes at 20 cm and the depth of
218 auger refusal - 108 cm at CFEMS, 190 at CFWMS, and 90 cm at CFRT. For each lysimeter, the
219 final auger bucket of the soil was retained, sieved to remove all coarse fragments greater than 2
220 mm in size, and mixed with DI water to create a slurry. That slurry was poured back into the
221 hole, after which the lysimeter was pushed in so that the slurry completely covered the porous
222 cup. The remaining fill material was sieved to remove coarse fragments greater than 2 mm, and
223 then tamped down around the lysimeter body to refill the hole in the order the soil was removed
224 from the ground.

225 Soil porewaters were collected at -50 kPa every three weeks from each lysimeter.
226 Samples were filtered with a 0.45-micron filter, an aliquot was acidified and stored in
227 refrigeration prior to analysis and another half was frozen. Acidified porewaters were analyzed
228 for geogenic cations on an ICP-OES (ThermoFisher ICAP 7400 ICP-OES, Thermo Fisher
229 Scientific, Waltham, MA, USA). Un-acidified porewaters were analyzed for Cl⁻, Br⁻, F⁻, and
230 SO₄⁻ on a Dionex 2100 Ion Chromatography System and were analyzed for NO₃⁻ N and NH₄⁺ N
231 using the Vn^{III} method (Doane and Horwath, 2003; Sims et al., 1995).

232 Porewaters accumulated in lysimeters for up to 24 hours. During that time, we assumed
233 they re-equilibrated with the atmosphere, degassing CO₂. Therefore, we used an equilibrium
234 calculation to determine DIC for the porewaters (Geochemist's Workbench[®] 12). To complete
235 the calculations, we assumed the alkalinity equaled the sum of the equivalents of strong base
236 cations minus the similar sum for strong acid anions and that the alkalinity and measured pCO₂
237 together determined the pH of the porewaters as calculated by GWB.

238 Additionally, The Geochemist's Workbench[®] 12 was used to calculate the chemical
239 equilibrium state for select soil porewaters using the porewater chemistry data and the measured

240 soil gas values – $p\text{CO}_2$ and $p\text{O}_2$. The equilibria at different depths at the three hillslope positions
241 over the sampling period were calculated to determine the porewater's saturation state with
242 respect to calcite. The equilibrium distribution of aqueous species and the saturation index of
243 various minerals, including calcite, were determined for each chemical system with enough
244 available chemical constraints, i.e., porewater cation and anion concentrations and $p\text{CO}_2$ and $p\text{O}_2$
245 values.

246 We also tracked soil moisture over the 2018 growing season using Stevens Hydra Probe
247 II soil moisture sensors (Stevens Water Monitoring Systems, Portland, OR, USA), installed at
248 10, 20, 40, and 90 cm below land surface in each soil pit. Measurements were recorded at 10-
249 minute intervals by Campbell Scientific CR1000 dataloggers (Campbell Scientific, Logan, UT,
250 USA) and transmitted via cellular telemetry.

251 2.5 Calculation of Carbonate Weathering due to Nitrification

252 To estimate the carbonate weathering from nitrification-associated acidity, we used a charge
253 balance approach (Perrin et al., 2008). We assumed that all Ca^{+2} and Mg^{+2} entered solution via
254 carbonate mineral weathering and all NO_3^- through nitrification of fertilizers and manure. This
255 allowed us to partition carbonate mineral weathering by the proportion of charge from Ca^{+2} +
256 Mg^{+2} balanced by $(\text{HCO}_3^- + \text{NO}_3^-)$ versus the remaining proportion balanced by HCO_3^- alone.
257 Concentration of these solutes in precipitation is at least one order of magnitude lower than soil
258 porewater concentrations (see supplementary table 3 for monthly averages from 2018
259 precipitation recorded at a nearby National Atmospheric Deposition Program site). At Cole
260 Farm, most N fertilization is achieved through the application of dairy manures. The organic N
261 in this manure is first converted to amines and urea (Eq. 2). The amines and urea are then

262 mineralized to produce NH_4^+ (Eqs. 3, 4, 5). Here, R is any complex organic molecule and R-
 263 $\text{CH}(\text{NH}_2)\text{COOH}$ refers to the N-containing component of the manure.



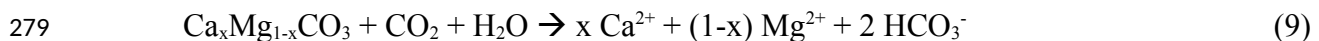
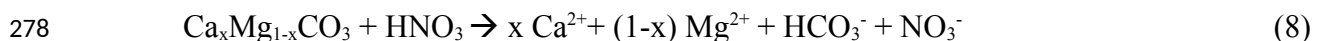
268 The ultimate products of this mineralization (NH_4^+) are oxidized to NO_3^- by chemo-
 269 lithoautotrophs (Eq. 6).



271 Summation and simplification of the hydrolysis of ammonia (Eq. 5) and nitrification of
 272 ammonium (Eq. 6) results in Equation 7.

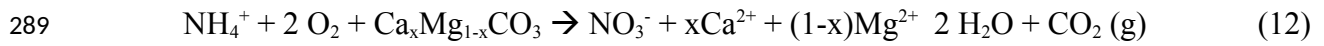
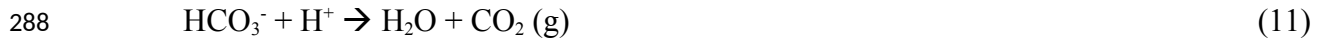
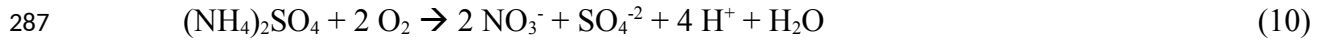


274 The nitric acid resulting from this reaction can drive down pH of the soil porewater
 275 and/or drive dissolution of minerals. The fastest dissolving minerals in sedimentary rocks such as
 276 those at Cole Farm are carbonates. Carbonate minerals (e.g., calcite, dolomite) readily dissolve in
 277 the presence of nitric acid (Eq. 8) in parallel to dissolution driven by carbonic acid (Eq. 9).



280 At Cole Farm the land managers also apply inorganic $(\text{NH}_4)_2\text{SO}_4$ to augment the applied
 281 manure. Again, the production of protons through nitrification of this fertilizer (Eq. 10) can
 282 result in low pH in soils, which can drive the bicarbonate produced in equation 8 to protonate
 283 and then ultimately degas if solubility of aqueous CO_2 is superceded. This happens when
 284 localized pH is less than about 6 (Stumm & Morgan, 1996; Eq. 11). Equation 12 is a summed

285 combination of equations 6, 8, and 11 that emphasizes that the reactions can act as a source of
 286 abiotic CO₂ to soil flux.



290 To calculate a rough estimate of the rate of dissolution of carbonate minerals by nitric
 291 acid, we estimated the nitric-generated carbonate weathering per month based on the
 292 concentration of nitrate in soil porewater, and the rate of porewater lost to groundwater for each
 293 month (Eq. 13).

$$294 \quad \sum_m^{\square} \text{ } \quad (13)$$

295 Here, m is the indicator for the month, $[x]_m$ is the soil porewater concentration of ion x (here,
 296 NO_3^-) for month m (mol L⁻¹), P is cumulative precipitation for month m measured at Cole Farm
 297 (m month⁻¹), I is the average fraction of precipitation that infiltrates to groundwater, here
 298 estimated as 0.5 (Li et al., 2017), and 10^3 is a factor to convert L to m³. This calculation results in
 299 CC_N , which is the annual carbonate weathering rate attributed to nitric acid (mol m⁻² yr⁻¹). This
 300 calculation is based on the assumptions of a soil profile experiencing no lateral transfer of
 301 solutes, all NO_3^- in solution balanced by Ca^{+2} or Mg^{+2} , and these cations entered solution through
 302 the weathering of carbonate minerals such that 1 mole of NO_3^- in solution has resulted in the
 303 dissolution of 1 mole of carbonate mineral (Eq. 8). However, there would be no impact on our
 304 estimates in the case of lateral transport of nitric acid and subsequent reaction with carbonate
 305 minerals in the pedon. Provenance of the acidity produced through nitrification is not important,
 306 as we are calculating the reaction of that acidity with the bedrock carbonates. However, if nitric
 307 acid reacted with carbonate minerals (or agricultural lime) upslope such that laterally flowing

308 porewaters containing Ca^{+2} and Mg^{+2} balanced by NO_3^- and HCO_3^- enter the subsurface of
309 CFEMS or CFWMS, our calculation would overestimate carbonate weathering due to
310 nitrification associated acidity.

311 This calculation is also based on the assumption that all NO_3^- in porewaters is derived
312 from nitrification and that the concentration of NO_3^- in porewaters on one day of the month is
313 representative of the concentration throughout the month. If porewater data were missing for a
314 month, values were interpolated between measured values.

315 2.6 Calculation of Carbonate Weathering by Carbonic Acid from Respired CO_2

316 We assumed that the remaining Ca and Mg in solution not balanced by $\text{HCO}_3^- + \text{NO}_3^-$ from
317 reaction of nitric acid with carbonate minerals and SO_4^{-2} from $(\text{NH}_4)_2\text{SO}_4$ fertilization is charge
318 balanced by HCO_3^- generated through carbonate weathering reactions (Eq. 9). While a small
319 amount of Ca- and Mg-containing silicate minerals are found in the bedrock, the most reactive
320 minerals by far are carbonates. The concentration of SO_4^{-2} in rainwater is at least an order of
321 magnitude lower than porewater concentrations (Supplementary Table 3) and S concentrations in
322 these soils is low such that pyrite oxidation is an unlikely source of acidity (Table 1). Therefore,
323 for CO_2 -driven dissolution of carbonates (Eq. 9), every mole of Ca + Mg in solution is balanced
324 by one HCO_3^- anion derived from CO_2 in the soil atmosphere and one derived from the mineral.
325 This is a reasonable assumption because Ca and Mg make up over 95% of the positive charge in
326 the porewaters, and NO_3^- and DIC make up over 95% of the negative charge. All HCO_3^- ,
327 including that derived from the respired CO_2 , exits the soil system as DIC rather than diffusing
328 from the soil surface as CO_2 gas, unless there is a significant shift in pH or temperature to cause
329 supersaturation. Thus, a downslope flux of DIC represents a sink for locally respired CO_2 and a
330 potential mechanism that could result in an $\text{ARQ} < 1$ in a particular pedon.

331 Based on the reaction stoichiometry of carbonate weathering, alkalinity of the deepest
332 lysimeter's porewaters at each hillslope position, and precipitation corrected for
333 evapotranspiration, we estimated the flux of respired CO₂ to the DIC pool at the three hillslope
334 positions (Eq. 14).

$$335 \quad \sum_m^m \dot{C}_c \quad (14)$$

336 Here CC_c is the carbonate weathering rate due to carbonic acid. Where porewater data were
337 missing for a month, they were interpolated. Monthly values were summed to estimate the flux
338 over the year.

339 2.7 Global Carbonate Stock Mapping

340 We sought to determine the distribution of soils across the globe that were likely to have 1) a
341 significant flux of respired CO₂ as DIC and 2) a significant gaseous flux of abiotic CO₂ to the
342 atmosphere due to carbonate weathering from nitrification associated acidity under low-pH
343 conditions. We mapped soil inorganic carbon stocks using the % mass of CaCO₃ in subsurface
344 soil (30 – 100 cm depths) from the World Inventory of Soil Emission Potentials (WISE30sec)
345 world soil database (Batjes, 2016). This database, which bins soil depths as surface (0 – 30 cm)
346 vs. subsurface (30 – 100 cm), estimates the CaCO₃ of the two soil depth intervals on the basis of
347 a 0.5 degree grid.

348 We then classified soils containing carbonates by binned subsurface (30 – 100 cm) soil
349 pH measured in an H₂O slurry, also from the WISE30sec database. We further parsed this
350 classification of soils as irrigated cropland, rainfed cropland, or non-cropland based on the 1 km
351 global grid from the Global Food Security Support Analysis Data (Thenkabail et al., 2016). We
352 used these datasets to classify carbonate-bearing soils into two types of soil as follows:

353 1) In neutral and basic soils, CO₂ is likely to dissolve because pH > 5.5. In these soils,
354 respired CO₂ may therefore be removed commonly from the soil atmosphere by dissolution into
355 porewater to form DIC, followed by porewater drainage. In this case, the CO₂ flux out of the soil
356 at the land surface is lower than the actual in situ soil respiration. For these soils, in situ
357 respiration rates are likely higher than measured gaseous CO₂ flux from the soil, confounding
358 ecosystem C budgets.

359 2) In acidifying soils (pH < 5.5) under agricultural land use that also contain carbonates
360 in the subsurface, nitrification of fertilizers and manures applied to these agricultural lands are
361 likely to dissolve carbonates while maintaining low pH in soil porewaters. This low pH favors
362 release of abiotic, carbonate-derived CO₂ into the gas phase. This abiotic source could increase
363 the surface soil CO₂ efflux (Zamanian et al., 2018, 2021) above that of soil respiration rates. For
364 these soils, measured CO₂ flux from the soil is higher than in situ respiration, again, confounding
365 ecosystem C budgets.

366 All mapping and raster analyses were performed in ArcMap (ArcMap Desktop Pro
367 version 10.7, ESRI, Redlands, CA).

368 2.8 Statistical Analysis

369 Statistical analyses were performed using R (R Core Team, 2019) software. Interpolation maps
370 were generated using the krig function in the fields package for R (Nychka et al., 2015). This
371 function was used to plot hand sampled gas measurements with depth over time. All
372 interpolations were created with the same parameters; l = 1, q = 50, covariance structure =
373 Mattern. Soil surface boundary conditions were set at 0.04% for the CO₂ interpolation, and
374 20.95% for the O₂ interpolation.

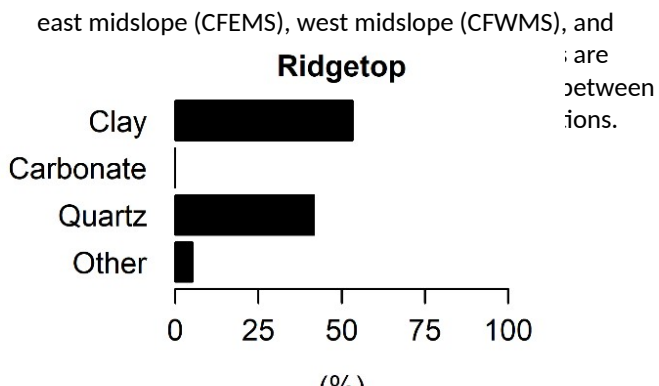
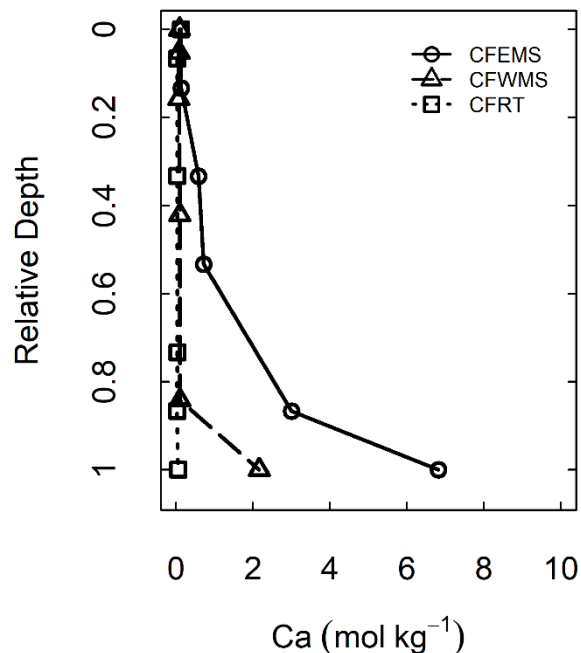
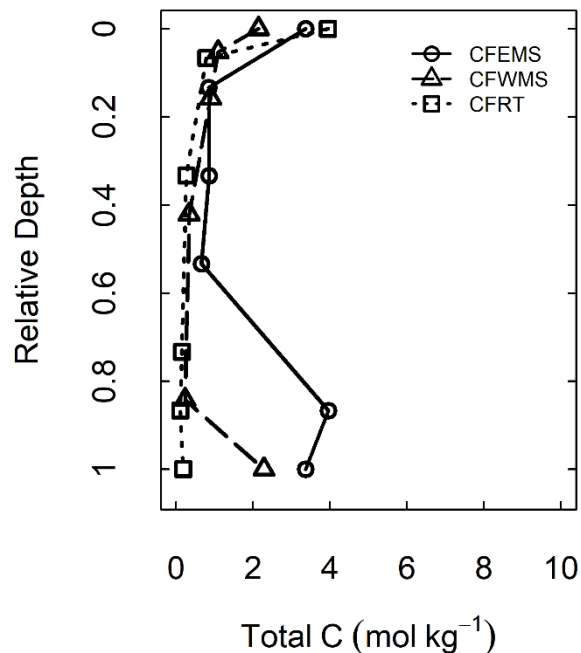
375 Lines of best fit for plots of $p\text{CO}_2$ versus $p\text{O}_2$ at each hillslope position were generated
 376 using the linear modeling (`lm`) function in R. Regression slopes at each hillslope position were
 377 tested for significant differences using the
 378 analysis of variance (`aov`) function in R. Slopes
 379 were determined to be significantly different if
 380 interactions between the independent variable
 381 (site position) with the covariate, $p\text{O}_2$, were
 382 significant. Repeated measures ANOVA were
 383 used to assess changes in $p\text{CO}_2$ and $p\text{O}_2$ over the
 384 growing season.

385 **3 Results**

386 3.1 Soil Elemental Analysis

387 Total elemental analysis by soil horizon and
 388 mineral composition of the C horizons of each
 389 hillslope position indicate soils of different
 390 elemental composition (Table 1, Fig. 2). Our
 391 results indicate that CFEMS is dominated by
 392 carbonate minerals in the soil subsurface.
 393 CFWMS consists of a mix of silicates and
 394 carbonates in the subsurface, and CFRT contains
 395 no carbonate minerals.

396 The most striking difference in base
 397 cation concentrations among the three soils



398 is the Ca concentrations (Fig. 2, Table 1). The
 399 markedly from CFEMS to CFWMS to CFRT,
 400 content inferred from XRD (Figure 3). Depth
 401 CFWMS soils increase from 0.34 wt. % to 8.6
 402 horizon sample at 190 cm. The largest increas
 403 soil profile at CFEMS between the BC and th
 404 concentrations than the WMS soils at all dept
 405 to 27.3% from the soil surface to the C horizo
 406 soils, the ridgetop does not have high Ca conc
 407 than increase with depth, Ca decreases from 0
 408 profile. Total C concentrations (Fig. 2) are consist
 409 cation concentrations at CFWMS and CFEMS are indicative of the concentrations of carbonate
 410 minerals. Total C concentration is high at the surface of all soil profiles, then it decreases below
 411 the surface sample before increasing again in the subsurface of CFWMS and CFEMS, but not
 412 CFRT. The mineral composition of the profiles confirms that the C at depth is associated with
 413 carbonate minerals (Fig. 3). Based on the XRD data, about 85% of the C horizon by mass at
 414 CFEMS consists of carbonate minerals. At CFWMS there is an equal mix of carbonates, layer
 415 silicates, and quartz, with each accounting for about 30% of the minerals present in the C
 416 horizon. At the ridgetop, carbonates were negligible and quartz and layer silicates comprise
 417 about 85% of the minerals (Fig. 3).

418 **3.2 Soil Moisture**
 419 Soil moisture differed at the three
 420 hillslope positions (Fig. 4). In

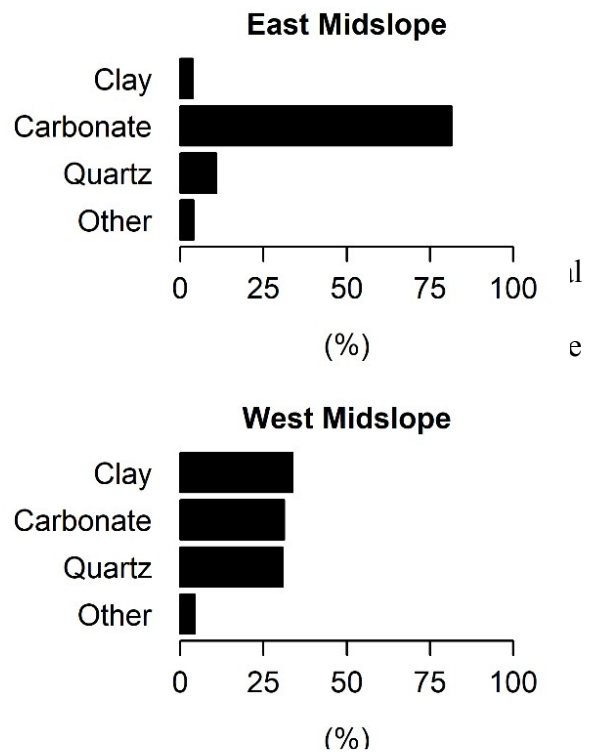
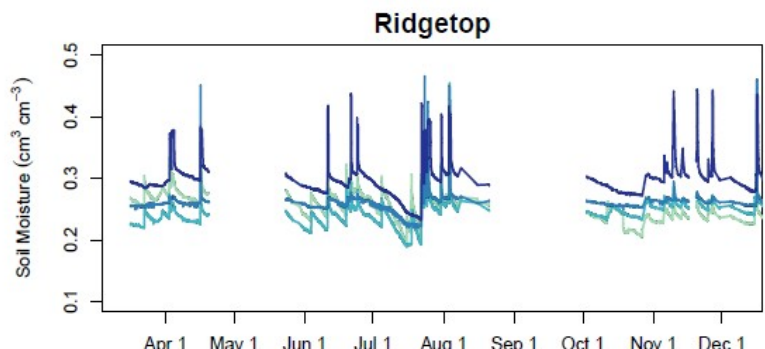
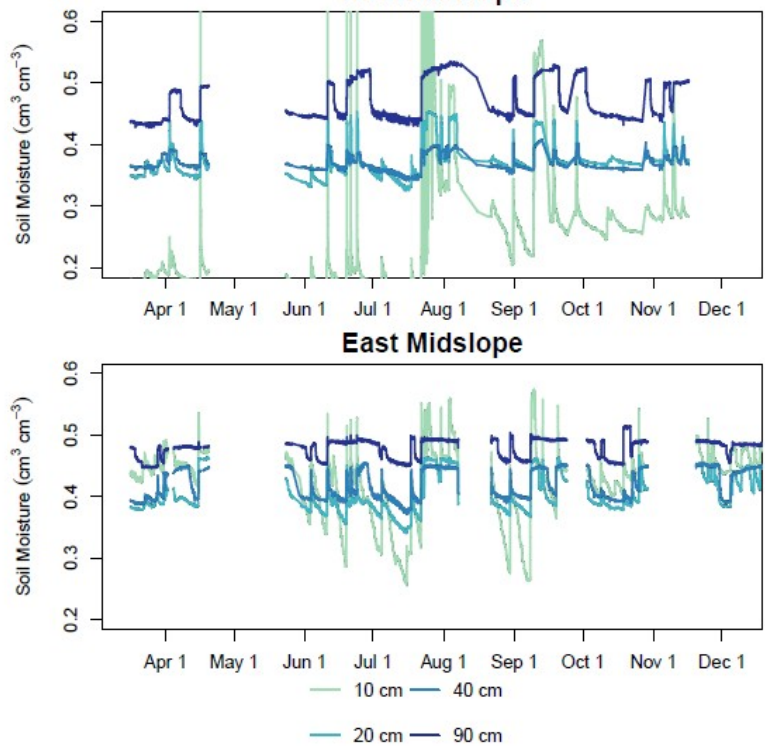


Fig 3: Distribution of minerals in the C horizons of the east midslope (CFEMS), west midslope (CFWMS), and ridgetop (CFRT) soils at Cole Farm.



421 general, the two midslope soils, CFEM
422 conditions than CFRT. Assuming the n
423 depth represents saturated conditions, t
424 subsurface (40 – 90 cm) through much
425 contrast, the CFRT soils did not mainta
426 (Fig. 4).



(CFRT), East Midslope (CFEMS), and West Midslope (CFWMS) at Cole Farm. Values are reported as volumetric water content.

Table 1: Elemental concentrations of soils (wt. % unless otherwise noted). Major element oxides and LOI sum to $100 \pm 2\%$

Site	Horizon	Depth (cm)	Al	Ca	Fe	K	Mg	Mn	Na	P	Si	Ti	LOI (900C)	S	Zr (ppm)	Sr (ppm)
West	Ap	0-10	5.12	0.34	4.29	2.6	0.77	0.1	0.26	0.11	29.6	0.6	10.3	0.03	270	bd*
Midslope						1		5				1				
West	Bt1	20-30	5.24	0.29	4.33	2.5	0.75	0.1	0.25	0.07	30.8	0.6	7.56	0.02	290	bd*
Midslope						8		8				4				
West	Bt2	30-40	4.75	0.27	3.93	2.2	0.63	0.1	0.30	0.07	32.4	0.6	6.88	0.01	310	bd*
Midslope						0		9				7				
West	Bt3	80-90	6.00	0.37	4.67	2.6	0.92	0.0	0.42	0.04	30.1	0.5	7.52	0.00	280	bd*
Midslope						1		9				3				
West	BC	160-170	6.28	0.39	5.33	3.2	1.16	0.1	0.30	0.07	29.3	0.5	6.61	0.01	290	bd*
Midslope						4		2				2				
West	C	190-200	6.32	8.65	4.31	3.6	1.25	0.0	0.19	0.05	21.4	0.4	14.4	0.01	160	170
Midslope						1		6				5				
East	Ap	0-10	5.36	0.52	4.35	2.9	0.89	0.0	0.17	0.10	28.1	0.5	13.6	0.05	250	bd*
Midslope						1		9				6				
East	Bt1	20-30	5.44	0.53	4.57	2.8	0.86	0.1	0.18	0.06	30.8	0.6	7.11	0.01	270	bd*
Midslope						1		1				2				
East	Btx	50-60	7.21	2.32	6.05	4.0	1.42	0.1	0.14	0.09	24.9	0.4	9.47	0.01	190	bd*
Midslope						0		2				6				
East	BC	80-90	7.94	2.87	3.39	5.0	1.30	0.0	0.18	0.07	25.9	0.5	7.51	0.01	190	bd*
Midslope						2		4				5				
East	C	130-140	4.23	12.0	5.68	2.2	2.78	0.1	0.10	0.07	16.5	0.2	20.8	0.01	170	250
Midslope						0		7				9				
East	C	150-160	1.43	27.3	3.85	0.7	2.01	0.1	0.06	0.06	6.50	0.1	34.2	0.01	78	760
Midslope						8		5				1				
Ridgetop	A	0-10	4.59	0.51	3.85	2.1	0.58	0.1	0.19	0.14	27.7	0.6	17.3	0.05	320	bd*
						9		9				1				
Ridgetop	AB	10-20	4.99	0.11	5.39	2.4	0.75	0.1	0.24	0.10	31.8	0.6	5.75	0.01	360	bd*
						2		8				3				
Ridgetop	Bt1	50-60	5.36	0.11	4.97	2.7	0.71	0.1	0.24	0.07	32.7	0.6	4.36	0.00	390	bd*
						9		0				4				
Ridgetop	Bt2	110-120	6.00	0.12	4.37	3.5	0.78	0.0	0.24	0.06	31.8	0.6	3.86	0.00	240	bd*
						8		1				2				
Ridgetop	C	130-140	8.18	0.10	4.88	5.2	1.07	0.0	0.14	0.03	27.5	0.6	4.58	0.00	190	bd*

Ridgetop	Cr	150-160	6.77	0.19	5.67	3 4.3 3	0.96	0.0 1	0.15	0.08	29.3	0 0.6 1	4.13	0.00	440	bd*
----------	----	---------	------	------	------	---------------	------	----------	------	------	------	---------------	------	------	-----	-----

*Below detection limit

428 3.3 Soil pCO₂ and pO₂

429 Soil pCO₂ at the three hillslope positions followed the same seasonal and depth trends but
 430 differed in concentration by hillslope position when controlling for sampling date and accounting
 431 for sampling depth (Fig. 5; $p < 0.001$). In the top 40 cm, we measured the highest pCO₂ in
 432 CFEMS, followed by CFWMS. CFRT showed a pCO₂ consistently lower than the two other
 433 hillslope positions. All three sites increased from a low concentration of pCO₂ around
 434 atmospheric levels at the beginning of the growing season in May to about 3% CO₂ at 40 cm
 435 depths in mid-August. However, the CFEMS soils reached higher pCO₂ earlier in the growing
 436 season than the CFWMS and CFRT soils (Fig. 5).

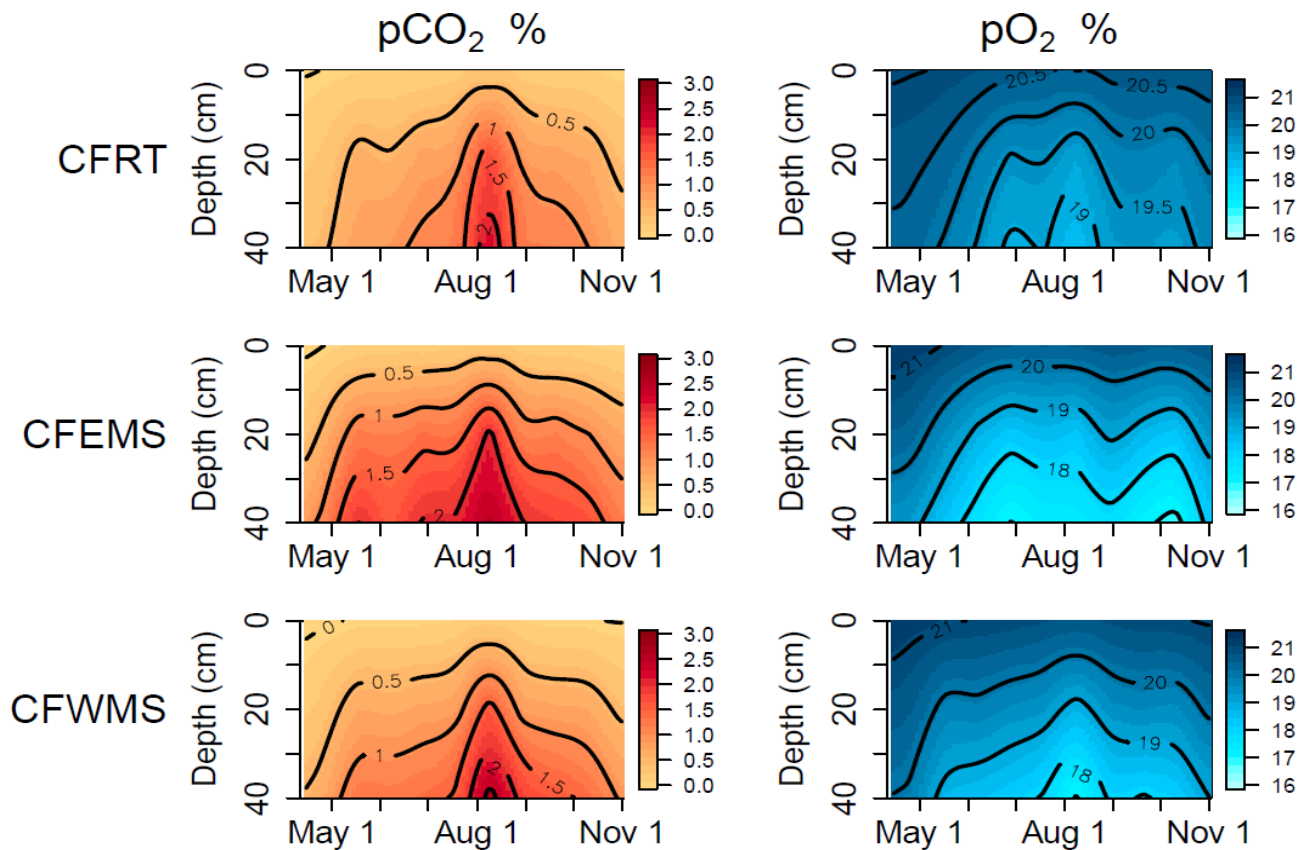


Fig. 5. Interpolated graphs of soil pCO₂ (%) and pO₂ (%) as a function of depth over the 2020 growing season in the top 40 cm of the east midslope (CFEMS), west midslope (CFWMS), and ridgetop (CFRT) soils. Darker orange indicates higher pCO₂. Lighter blue represents lower pO₂.

437 Soil pO₂ also differed by hillslope position when controlling for sampling date and depth
 438 (Fig. 5, p = 0.004). The CFEMS and CFWMS pO₂ was lower than that of CFRT. All three soils
 439 experienced lowest pO₂ in August. While CFRT reached a low around 17%, CFEMS and
 440 CFWMS reached a low around 16%. At all hillslope positions soil pO₂ decreased from around
 441 atmospheric concentrations in April to a low in August and September. The low pO₂ in the soil
 442 subsurface lasted longer than the high of pCO₂ (Fig. 5)

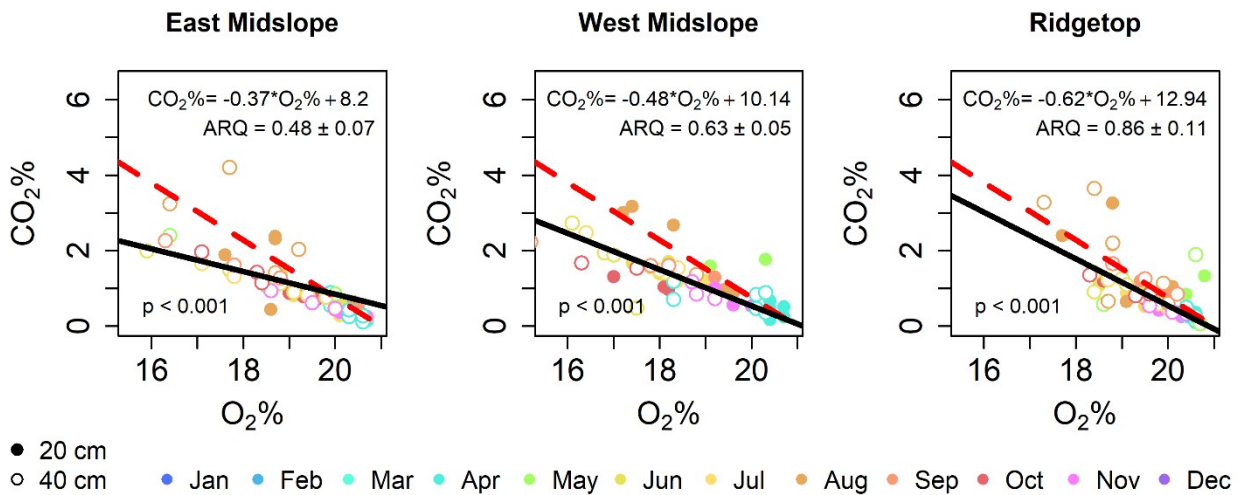


Fig 6: Plots of pO₂ vs. pCO₂ from 20 and 40 cm gas wells in the Cole Farm soils during the 2018 growing season. The dashed line represents the theoretical relationship between pO₂ and pCO₂ governed by aerobic respiration and diffusion (ARQ=1). The solid black line and the equation at the bottom of each plot represents the regression line of best fit through the gas data. Open circles represent samples collected from 40 cm and closed circles are samples collected from 20 cm.

443 Regressions of soil pCO₂ vs. pO₂ differ by hillslope position (Fig. 6). The ANCOVA of
 444 soil pCO₂ vs. pO₂ by hillslope position (for 20 cm and 40 cm depths), yields regression slopes for
 445 CFEMS (-0.37 ± 0.05) and CFWMS (-0.48 ± 0.04) soils that differ significantly (p < 0.01) from
 446 the CFRT soil (-0.65 ± 0.08). Likewise, the CFEMS and CFWMS regressions are significantly
 447 different from the slope of -0.76 that is consistent with aerobic respiration (+diffusion). The
 448 dominant ARQs consistent with the slopes for CFEMS, CFWMS, and CFRT are 0.48 ± 0.07,

449 0.63 ± 0.05 , and 0.86 ± 0.11 , respectively. The regression slopes and ARQs for CFEMS and
450 CFWMS are consistent with processes that lower the concentration of CO_2 in the gas phase
451 compared to O_2 in comparison to the ratios expected based on aerobic respiration (Hodges et al.,
452 2019).

453 3.4 Soil Porewater Chemistry

454 Concentrations of geogenic cations in porewater solutions varied by hillslope position and time
455 over the 2018 growing season (Fig. 7). In general, the solute concentrations in CFEMS and
456 CFWMS porewaters were higher than the CFRT porewaters; for example, [Ca] and [Mg] were
457 higher in the near-swale soils than the ridge soils. Additionally, [Ca] and [Mg] increased over the
458 growing season but were generally higher in the deep lysimeters than in the shallow lysimeters
459 year-round. On the other hand, Si concentrations did not vary by hillslope position and were
460 higher in the surface than subsurface. The concentrations of Na and K in general were also
461 higher in CFWMS and CFEMS than CFRT throughout the growing season.

462 Anion concentrations in the lysimeters also varied by hillslope position throughout the
463 2018 growing season (Fig. 7). In general, all anions were higher in concentration in the
464 subsurface of CFWMS and CFEMS than at the surface or at any depth at CFRT. In the
465 subsurface of CFWMS, NO_3^- - N was around 4 ppm and was consistently highest throughout the
466 growing season, followed by CFEMS which increased from around 1.5 ppm to 4.5 ppm in
467 August. On the other hand, CFRT NO_3^- - N was consistently lower than the other two sites,
468 around 1 ppm throughout the growing season. Surface concentrations of NO_3^- - N were in
469 general lower than in the subsurface, except at CFEMS in July and August.

470 Alkalinity, pH, and calcite saturation index calculated with GWB varied by pedon (Table
471 2) following the differences in measured porewater anions and cations and mineralogy.

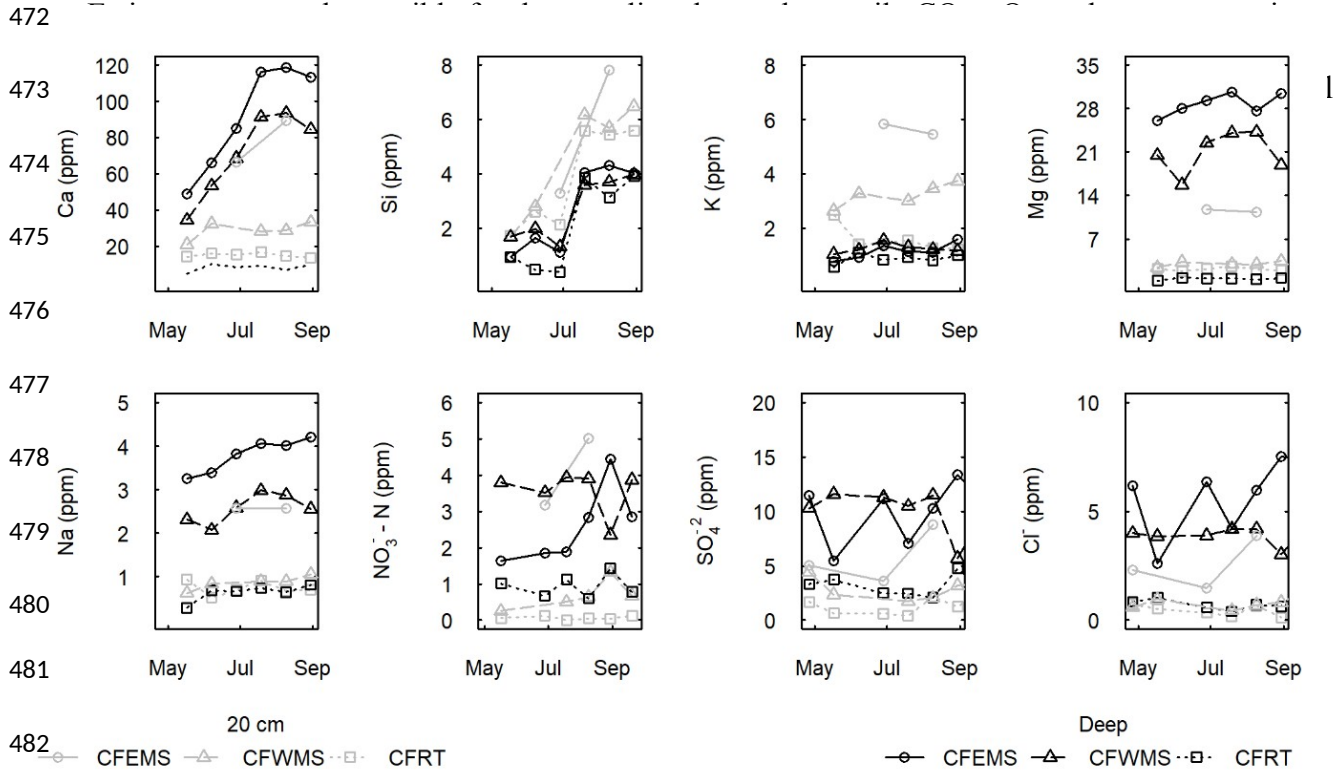


Fig 7: Major solute concentrations in soil water collected from lysimeters at east midslope (CFEMS), west midslope (CFWMS), and ridgetop (CFRT) soils over the 2018 growing season. Gray represents 20 cm lysimeters and black represents subsurface lysimeters at 108, 190, and 90 cm at CFEMS, CFWMS, and CFRT, respectively.

(CFEMS)			8/9/2018	4.76	6.98	0.06 oversat
	108	X	5/17/2018	4.41	7.18	-0.02 eq
		X	7/19/2018	8.05	7.19	0.57 oversat
West Midslope (CFWMS)	20		5/17/2018	1.23	7.04	-0.98
			7/19/2018	1.67	7.11	-0.66
			8/9/2018	1.68	6.65	-1.11
			8/30/2018	1.89	7.47	-0.20
Ridgetop (CFRT)	20		6/28/2018	0.81	6.68	-1.64
			7/19/2018	0.96	6.94	-1.28
			8/9/2018	0.81	6.38	-1.97
			8/30/2018	0.76	6.92	-1.48
	90		6/28/2018	0.41	6.32	-2.53
			7/19/2018	0.42	6.48	-2.34
			8/9/2018	0.33	5.86	-3.17
			8/30/2018	0.39	6.28	-2.54

484 3.5 Estimates of Carbonate Weathering due to Nitrification and Carbonic Acid
485 At CFEMS, CC_N was estimated at the rate of about $0.27 \text{ mol carbonate m}^{-2} \text{ yr}^{-1}$. Accounting for
486 $CC_N + CC_C$ (i.e. total carbonate dissolution), weathering due to nitrification associated acidity
487 accounts for 5.4% of all carbonate dissolution at the CFEMS position. At CFWMS, because
488 there is a higher concentration of NO_3^- over much of the growing season and a lower
489 concentration of Ca and Mg (consistent with the lower carbonate mineral abundance), CC_N was
490 estimated at about $0.39 \text{ mol m}^{-2} \text{ yr}^{-1}$ and this accounts for 11% of all carbonate weathering. The
491 calculated pH of the porewaters at the midslopes is higher than 6 (Table 2). Our calculations
492 indicate that NO_3^- in the carbonate-derived soils promotes carbonate dissolution but not a
493 gaseous CO_2 flux, because of the high pH that is maintained. Therefore, while weathering of
494 carbonate minerals by nitric acid may on occasion drive CO_2 into the gaseous phase in
495 microsites, the generally higher pCO_2 and buffering capacity of the carbonate rocks favors
496 dissolution of CO_2 in porewaters and loss of C from the soil as HCO_3^- (Gandois et al., 2011).
497 Therefore, we estimate that there is no abiotic gaseous CO_2 flux from the reaction of carbonate
498 minerals with acidity produced through nitrification in any of the Cole Farm soils.

499 We also calculated the rate of reaction of carbonate minerals in the soil with carbonic
500 acid (CC_C). At CFEMS, the soil with the highest carbonate content, CC_C consumes about 60 g C
501 $\text{m}^{-2} \text{ yr}^{-1}$ of respired CO_2 . In the soils of CFWMS, CC_C consumes respired CO_2 at the rate of 41 g
502 $\text{C m}^{-2} \text{ yr}^{-1}$. These correspond to weathering rates of carbonate minerals due to carbonic acid of
503 5.0 and $3.5 \text{ mol carbonate m}^{-2} \text{ yr}^{-1}$ at CFEMS and CFWMS, consistent with the higher abundance
504 of carbonate minerals in CFEMS.

505 It should be noted that these calculations only account for reactions to the depth of the
506 deepest lysimeter at 108 cm and 190 cm at CFEMS and CFWMS, respectively. These deep
507 lysimeters are installed below the carbonate reaction fronts at the two sites and therefore

508 represent the interaction of porewaters with the carbonate minerals at CFEMS and CFWMS
509 (Figs 2, 3; Table 1). Oversaturation of the lysimeter at 20 cm in the former soil likely is related
510 to the occasional liming of the soils by past land managers.

511 3.6 Global Carbonate System Reactions

512 Maps of the carbonate-bearing soils (adapted from Batjes, 2016; and Thenkabail et al., 2016)
513 represent lands in which carbonate minerals could affect soil CO₂ flux as discussed previously
514 (Fig. 8). Soils that contain carbonate minerals and are neutral to basic represent about 98 million
515 km² out of the global land area of 148 million km² (Fig. 8a). These soils favor inorganic carbon
516 in the aqueous phase and could therefore lose dissolved C as a large fraction of soil respiration.
517 Acidic agricultural soils that contain carbonate minerals represent about 7.4 million km² (Fig.
518 8b). Nitrification in these soils could support carbonate weathering (Eq. 2) and release CO₂ in the
519 gas phase from the protons produced if pH were maintained low enough (Eq. 3).

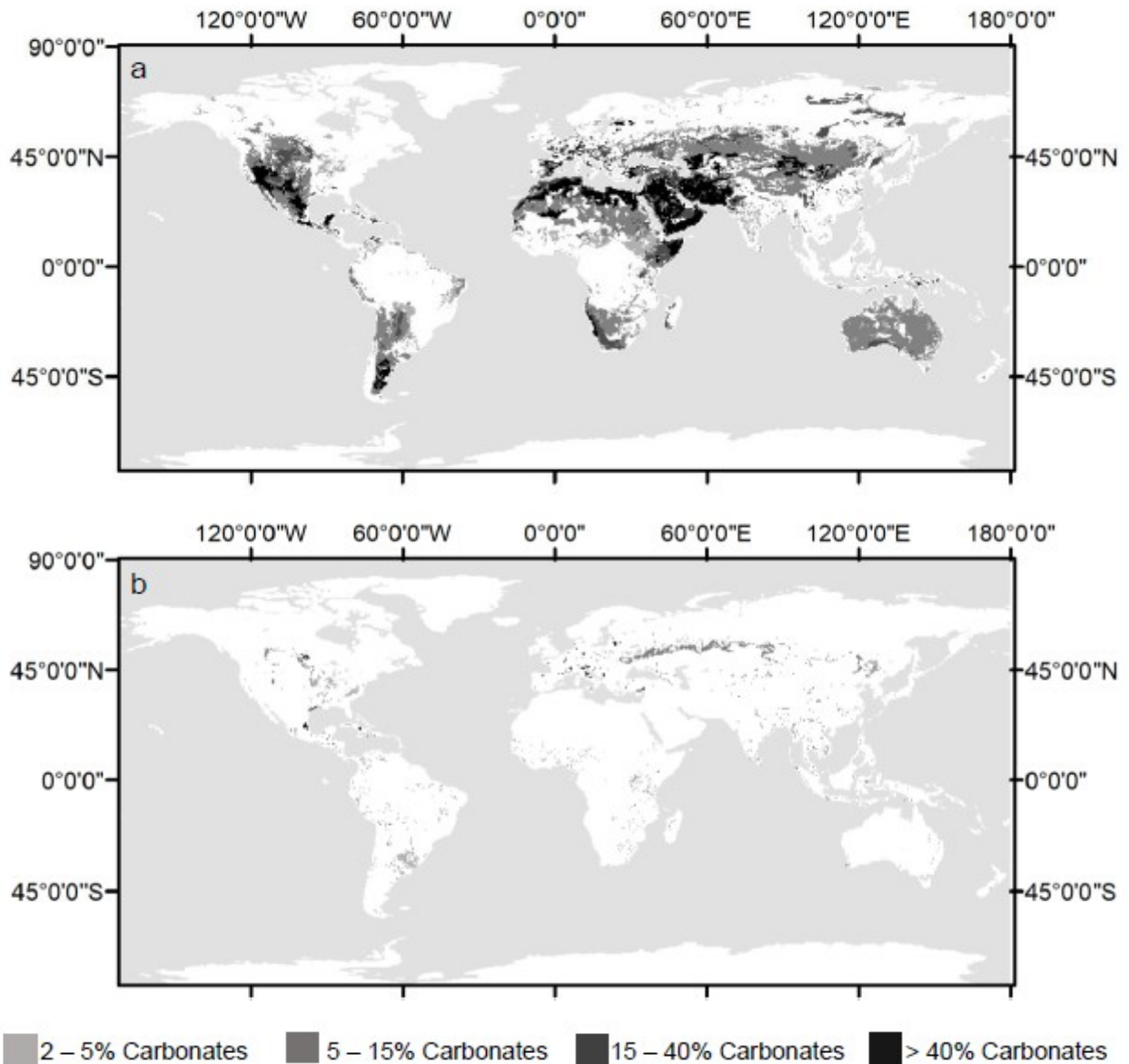


Fig 8: Soils with carbonates in the subsurface (30 - 100 cm) on a 0.5 degree raster grid classified by pH and land use. Darker cells indicate higher percent carbonates. The two panels represent different carbonate system processes that could affect soil CO₂ flux measurements and obscure interpretations of soil respiration rates. a) soils highlighted in this map represent neutral and basic soils underlain by carbonates. Conditions in these soils favor dissolution of respired CO₂ (and a lower CO₂ flux) and would result in underestimation of soil respiration rates b) soils highlighted in this panel represent acidic agricultural soils (pH < 5.5) with subsurface carbonates. Nitrification in these soils from application of fertilizers and manures may increase acidity and drive inorganic carbon into the gas phase. This would increase abiotic sources of CO₂ flux and lead to overestimates of soil respiration, if only surface CO₂ flux were measured.

521 **4 Discussion**

522 In support of hypothesis 1, our results show that hillslope position affects soil pCO₂, and this is
523 largely due to differences in soil moisture conditions. The hillslope positions (CFEMS and
524 CFWMS) with the highest soil moisture generated the highest pCO₂ over the 2018 growing
525 season. Our results are consistent with other findings of soil moisture effects on respiration;
526 higher soil moisture without prolonged saturation favors high root and microbial respiration rates
527 and restricts diffusion of the CO₂ out of the soil profile (Brook et al., 1983; Hasenmueller et al.,
528 2015; Pacific et al., 2010; Raich & Schlesinger, 1992). However, these soil moisture differences
529 by hillslope position are not solely responsible for the variation in pCO₂ and pO₂ we observed at
530 Cole Farm. The ARQ at the two calcareous soils was significantly less than 1, while the soil
531 without carbonates indicated an ARQ of 1. Below we suggest that this difference in ARQ is
532 likely due to the interaction of soil moisture with carbonate minerals at the midslopes (noting the
533 lack of carbonates in the ridgetop soils). These interactions resulted in a greater proportion of
534 respired CO₂ partitioned into the aqueous phase, supporting hypotheses 2 and 3. We also suggest
535 that there is little evidence supporting hypothesis 4; i.e., carbonate weathering from nitrification
536 acidity is not a source of gaseous CO₂ at our site.

537 4.1 Carbonate Mineralogy Affects Soil ARQ at Cole Farm Midslopes

538 The ARQ of ~1 at CFRT indicates that aerobic respiration and diffusion of CO₂ and O₂ are the
539 dominant controls on soil pCO₂ at the ridgetop hillslope position where carbonates are largely
540 lacking (Angert et al., 2015; Hodges et al., 2019). In contrast, at the midslopes, the ARQs are
541 significantly less than 1, and these values indicate that aerobic respiration and diffusion are not
542 the only controls on soil pCO₂. This points to the prevalence of a process that draws soil O₂ or
543 CO₂ out of the gas phase. There is either less CO₂ in the gas phase than one would assume from
544 the O₂ consumed in aerobic respiration, or there is less O₂ in the gas phase than one would

545 predict from the CO₂ produced via respiration. Here, we systematically examine these potential
546 reactions and conclude that DIC export is the most likely cause for low ARQ in our midslope
547 soils.

548 Nitrification by chemo-lithoautotrophs (Tsutsui et al., 2015) or metal oxidation (Hodges
549 et al. 2019) can decrease O₂ to cause ARQ < 1, but our data enable us to rule out the possibility
550 that these processes consume enough soil O₂ to shift ARQ at our sites. From our porewater NO₃⁻
551 concentrations, using the same estimation technique outlined in the methods section (Eq. 13),
552 and based on the stoichiometry of nitrification (Eq. 6), we estimated that nitrification would
553 remove about 4.5 g O₂ m⁻² yr⁻¹. To shift the ARQ to a value comparable to our observations,
554 nitrification rates would need to be two orders of magnitude greater, consuming about 450 g O₂
555 m⁻² yr⁻¹. In forest soils of humid, temperate regions, oxidation of metals (mostly Fe) has also been
556 pointed to as a potential mechanism of low ARQ (Angert et al., 2015; Hodges et al., 2019; Kim
557 et al., 2017). However, total Fe concentrations at the three hillslope positions are similar (Table
558 1), and so one would expect an oxidation signature to be consistent at the three sites, rather than
559 different. In fact, accounting for the differences in soil moisture, we would anticipate an
560 oxidation signature (ARQ < 1) at CFRT and a reduction signature (ARQ > 1) at the midslopes;
561 this is not what our measurements show.

562 If removal of gaseous O₂ is not driving low ARQ at our midslope sites, then a reaction
563 that reduces soil pCO₂ must be at play, and we calculate that this “missing” CO₂ represents a
564 substantial C flux in soils. The deviation of the midslope pCO₂-pO₂ regressions (Fig. 6) from
565 slopes reflecting an ARQ of 1 represent C missing from the gaseous phase (Eq. 15; Sánchez-
566 Cañete et al., 2018). At Cole Farm, we take the slope of -0.65, the regression slope at CFRT, to
567 represent the aerobic baseline for the watershed (i.e. ARQ=1).

$$568 \quad \frac{\text{Actual Slope}}{\text{Aerobic Slope}} = \frac{\frac{\Delta CO_{2\text{Actual}}}{\Delta O_{2\text{Actual}}} * \Delta O_{2\text{Aerobic}}}{\Delta CO_{2\text{Aerobic}}} = \frac{\Delta CO_{2\text{Actual}}}{\Delta CO_{2\text{Aerobic}}} = C_p \quad (15)$$

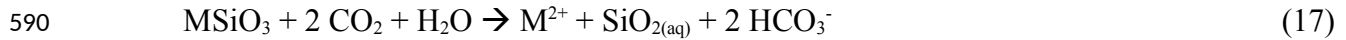
569 Here we define ΔCO_2 as the change in pCO_2 for unit change of pO_2 . If we assume that all
 570 deviation in the regression slope is due to a change in pCO_2 and not pO_2 , then ΔO_2 , which is the
 571 unit change of pO_2 for a change in pCO_2 , of the actual slope and aerobic slopes cancel out.
 572 Therefore, the ratio of the actual slope to the slope that represents aerobic respiration plus
 573 diffusion gives us the fraction of CO_2 lost per unit change in O_2 for the measured soil compared
 574 to the aerobic soil here called C_p (Eq. 15). Therefore, one minus C_p yields the fraction of CO_2 loss
 575 missing from the measured soil, here C_m (Eq. 16).

$$576 \quad 1 - C_p = C_m \quad (16)$$

577 Once we calculate C_m we can then multiply it by the gaseous CO_2 flux for a similar site
 578 that we know is dominantly controlled by aerobic respiration and diffusion, and this will allow us
 579 to estimate the ‘missing’ gaseous CO_2 flux from Cole Farm. We know that about 1500 g C m^{-2}
 580 yr^{-1} is the simulated root plus heterotrophic soil respiration rate of a nearby site where soil CO_2
 581 flux is largely controlled by aerobic respiration and diffusion (Shi et al. 2018; Hodges et al.,
 582 2019). Therefore, using equations 15 and 16, and then multiplying C_p by 1500 g C m^{-2} , we
 583 estimate that 43% of the respired carbon or $645 \text{ g C m}^{-2} \text{ yr}^{-1}$ is missing from the gas phase flux at
 584 CFEMS and 26% or $390 \text{ g C m}^{-2} \text{ yr}^{-1}$ is missing at CFWMS.

585 4.2 Where Is the “Missing” CO_2

586 At least three processes may account for the “missing” soil CO_2 that leads to $ARQ < 1$ at our
 587 midslope sites: silicate weathering, carbonate weathering, or CO_2 dissolution in soil water.
 588 Silicate minerals (here shown generically as $MSiO_3$) participate in acid-base weathering
 589 reactions with DIC (Eq. 17), and if the DIC is removed in drainage, can represent a CO_2 sink.



591 We can rule out this process because dissolution rates of the silicate minerals in shales of central
592 Pennsylvania are sufficiently slow that they have a negligible effect on soil pCO_2 at the temporal
593 resolution of our sampling (Hodges et al., 2019; Jin et al., 2014). Similarly, when we calculated
594 (see methods and results) CO_2 -generated carbonate weathering reactions at the midslopes, we
595 observed that this would lower the gaseous CO_2 flux by 60 and 41 $\text{g C m}^{-2} \text{yr}^{-1}$ at CFEMS and
596 CFWMS.

597 Thus, the last process that could account for the “missing” CO_2 from our midslope
598 profiles is CO_2 dissolution into porewaters and removal from the profile as DIC. Several lines of
599 evidence suggest that this is the most likely mechanism causing low ARQ in our midslope
600 profiles. The abundance of carbonate minerals, which buffer soil pH, along with high soil
601 moisture at these locations favor CO_2 dissolution and limit CO_2 diffusion out of the soil (Pacific
602 et al., 2010). However, high soil moisture alone cannot account for the observed differences in
603 ARQ. Saturated soil conditions without significant export would favor anaerobic respiration and
604 therefore an $\text{ARQ} > 1$, as wet soils limit O_2 diffusion and necessitate soil microbes to switch to
605 alternate terminal electron acceptors (Hodges et al., 2019). It is the interaction of high soil
606 moisture, efficient drainage, and mineralogy that enables high porewater pH and high
607 throughflux of water, which in turn increases the solubility of CO_2 in the porewater and loss of
608 DIC from the soil. The calculations in the results reflect this conclusion, as we found the greatest
609 deficit of respired CO_2 and highest carbonate weathering rate at CFEMS, the soil with the
610 highest carbonate mineral abundance.

611 These findings support hypothesis 2, as the carbonate mineralogy of the midslope soils
612 acts to facilitate the partitioning of respired CO_2 into DIC, some of which is transported deeper

613 and farther downslope or into deep groundwater. We are not the first to interpret a CO₂
614 dissolution signature from low ARQ. Olshansky et al. (2019) found that dissolution of soil CO₂
615 reduced soil CO₂ flux into the atmosphere by over half in a subhumid watershed underlain by
616 metamorphic rocks. Additionally, Angert et al. (2015) reported ARQ values below 1 in
617 calcareous soils in a Mediterranean climate that they attributed to CO₂ dissolution and carbonate
618 weathering. However, while others have invoked CO₂ dissolution as the cause of ARQ < 1
619 (Angert et al., 2015; Olshansky et al., 2019; Sánchez-Cañete et al., 2018), we are the first to
620 document such a pattern in a humid, temperate system. Our results indicate DIC export could be
621 relevant in a range of ecosystems, as discussed in the section “*Extrapolating these Results*
622 *Globally.*”

623 Our findings that a large proportion of respired CO₂ exports as DIC from the midslope
624 soils of Cole Farm is comparable to other works. For example, a column experiment of dolomitic
625 soils underlain by dolomite gravels found that respired C could account for 90 – 100% of the
626 DIC that eluted from the column base. Like our findings at the midslopes, this study also found
627 increased DIC export with both increased pCO₂ and soil moisture (Schindlbacher et al., 2019).
628 Furthermore, Kindler et al. (2011) found that DIC export accounted for 25% of total C flux in a
629 forest with a calcareous subsoil. This DIC export to groundwater serves as a temporary sink for
630 respired C, perhaps for hundreds to thousands of years (Hamilton et al., 2007; Sanderman, 2012).
631 However, this DIC likely degasses once it enters streams and rivers, changing the time and place
632 of the eventual CO₂ efflux (Butman & Raymond, 2011). Our results underline that partitioning
633 of respired C to the aqueous phase represents an important C flux that should be accounted for
634 when measuring soil C fluxes and accounting for watershed C balance.

635 4.3 Nitric Acid Has a Negligible Effect on ARQ and Partitioning of CO₂
636 We also explored the role of nitric acid-promoted carbonate weathering in driving carbonate-
637 derived CO₂ into the gaseous phase. While our calculations show that NO₃⁻ in the porewaters is
638 associated with carbonate dissolution, both the ARQ at the midslope soils and our calculations
639 show that the contribution of these reactions to gaseous CO₂ flux is negligible to non-existent.
640 The soil atmosphere in the carbonate-bearing soils at Cole Farm show a lack, not a surplus, of
641 gaseous CO₂ relative to O₂. Our results refute hypothesis 4 since our results did not indicate
642 gaseous CO₂ release from nitrification-associated carbonate weathering.

643 Our findings are comparable to those found by others working in agricultural systems
644 underlain by carbonate-bearing rocks. For example, Perrin et al. (2008) found that N fertilization
645 resulted in a higher proportion of stream cations balanced by NO₃⁻ than HCO₃⁻. They estimated
646 that this NO₃⁻ replaced 7-17% of the HCO₃⁻ in rivers, comparable to our estimates from lysimeter
647 samples at CFEMS and CFWMS. A follow-up study to Perrin et al. indicated that the acidity
648 from nitrification did not lower soil pH sufficiently in carbonate systems to drive carbonate-
649 derived CO₂ into the gas phase (Gandois et al., 2011). Likewise, in laboratory column
650 experiments, Song et al. (2017) found that all ammoniacal fertilizers increase carbonate
651 weathering rates compared to organic N or urea, but that they do not sufficiently lower pH to
652 drive CO₂ into the gaseous phase.

653 However, some workers have estimated large abiotic CO₂ fluxes associated with
654 nitrification in agricultural systems (Zamanian et al., 2018, 2021). The key difference between
655 our results and those of Zamanian et al. (2018) are that Zamanian et al. (2018) assume that all
656 nitrate-promoted weathering reactions result in CO₂ in the gaseous phase. In reality, soil
657 moisture, pH, temperature, and distribution of carbonates in the soil profile determine whether a
658 gaseous CO₂ flux is a reasonable outcome from the weathering of carbonates by nitrification

659 associated acidity. More specifically, this gaseous CO₂ flux is only reasonable if there is a high
660 rate of nitrification and a small amount of carbonate minerals present such that the acid input
661 outstrips the capacity of carbonate minerals to buffer solution pH. Indeed, Hamilton et al. (2007)
662 found that reaction of carbonic acid derived from root and microbial respiration with agricultural
663 lime far outpaces the generation of CO₂ caused by nitric acid reacting with carbonate minerals.
664 West & McBride (2005) estimated that about 40% of C in agricultural lime eventually degasses
665 from soils or riverine systems. Contrary to the hypothesis of Zamanian et al. (2018), the results
666 of Hamilton et al. (2007) and West & McBride (2005) together suggest that agricultural lime has
667 either a net-zero impact on CO₂ efflux or acts as a small C sink. Thus, our results and the work of
668 others call for a nuanced approach when estimating effects of N fertilization on carbonate
669 weathering and potential gaseous CO₂ emissions from nitrification-associated acidity reacting
670 with carbonate-bearing minerals.

671 4.4 Extrapolating These Results Globally

672 Clearly DIC loss in the aqueous phase represents an important component of soil C flux in many
673 systems, and this partitioning between gaseous and aqueous phases is not yet appreciated in
674 short-timescale C cycle modeling. In this section we explore the potential global significance of
675 the reactions we have detailed in this discussion with a mapping exercise.

676 Soil inorganic C (SIC) comprises over one third of the global soil carbon pool and it may
677 be particularly sensitive to changes in land use and climate (Ahmad et al., 2015; Bargrizan et al.,
678 2020; Zamanian et al., 2016). Reactions of SIC in the soil system have disparate effects on soil
679 CO₂ flux, and those effects are difficult to parse by magnitude and scale. Therefore, we mapped
680 the global distribution of carbonate-bearing soils likely affected by the reactions we explored at
681 Cole Farm. First, we mapped soils in which CO₂ dissolution into soil water that leaves the soil

682 acts as a sink for gaseous CO₂, lowering soil CO₂ fluxes (Fig. 8a). Second, based on the slow rate
683 of nitrification-induced weathering at Cole Farm, we modified the mapped soils in Zamanian et
684 al. (2018) to sites we think may actually have an abiotic soil CO₂ flux due to nitric acid from
685 fertilizers that dissolve carbonate minerals and decrease the soil pH to favor an efflux of CO₂
686 into the gaseous phase (Fig. 8b).

687 At about 98 million km², the carbonate-bearing soils that we hypothesize will lose
688 respired C through CO₂ dissolution in porewaters and weathering reactions represent far greater
689 land area than the 7.4 km² of agricultural soils with N fertilization and acidic pH. Based on our
690 work and others, dissolution of respired CO₂ in carbonate-bearing soils with neutral and basic pH
691 can reduce soil CO₂ flux by over one half (Olshansky et al., 2019; Sánchez-Cañete et al., 2018);
692 DIC export from many of these carbonate systems may represent a large C export from soils
693 during the growing season (Kindler et al., 2011), or after extreme precipitation events (T. Liu et
694 al., 2018b). In fact, some soils show decreasing pCO₂ with depth at the deepest depths, consistent
695 with drawdown by drainage of DIC (Brantley et al., 2014; Stinchcomb et al., 2018). This loss of
696 DIC derived from mineral weathering is a sink for respired C (Bargrivan et al., 2020).

697 While dissolution of respired CO₂ may be predominant in these soils, much of this land
698 area is desert in which soil respiration and moisture are low. Therefore, the effect of this desert
699 land on the global carbon cycle is minor. However, as rainfall or irrigation increases soil
700 moisture, more CO₂ dissolves in porewaters to weather carbonate minerals (Kim et al., 2020;
701 Raza et al., 2020). Even in the desert soils in dry lands, eddy covariance flux studies have
702 documented anomalous CO₂ consumption. For example, Wolfahrt et al. (2008) found large
703 annual CO₂ uptake rates in the Mojave Desert. After review, most attribute such C uptake in
704 cases like those described by Wolfahrt et al. (2008) to carbonate mineral dissolution (Cueva et

705 al., 2019; Kowalski et al., 2008; Rey, 2015; Serrano-Ortiz et al., 2010). Evidence of the
706 significance of dissolved inorganic carbon fluxes in these soils from across a range of
707 ecosystems underlines that DIC and carbonate system reactions must be accounted for when
708 constructing watershed carbon budgets.

709 On the other hand, acidic agricultural soils that also contain carbonates cover 7.4 million
710 km², or about 4.6% of the terrestrial surface area of the earth. While these soils are scattered,
711 there are large pockets in centers of agricultural production within Canada, the United States,
712 Uruguay, Argentina, Western Europe, and Russia (Fig. 8b). It is in these soils that we may
713 expect to observe an increase in soil CO₂ flux from nitrification-derived acidity enhancing
714 carbonate weathering. This estimated land area is much less than previous estimates of
715 nitrification-affected carbonate soils (Zamanian et al., 2018) because we only mapped soils with
716 a pH < 5.5 that would favor CO₂ in the gas phase. For other neutral and basic soils where nitric
717 acid weathering occurs, it is likely that the abiotically released CO₂ remains dissolved in soil
718 water. Even in the warm, acidic soils in which gaseous CO₂ is most favored, and at the highest
719 range of estimated CO₂ production from proton-promoted carbonate dissolution in Zamanian et
720 al., (2018), the CO₂ flux would only be 5 g C m⁻² yr⁻¹. While potentially important in certain
721 cases, it is likely within error of most watershed C budget studies.

722 However, our maps do not provide a complete picture of the potential soils affected by
723 the two scenarios outlined above. The resolution of figure 8, and even the USDA soil survey, do
724 not allow prediction of the extent of variability in soil mineralogy as that which we observed at
725 Cole Farm. This highlights the importance of such mineralogical and elemental analyses of soils
726 when conducting ecosystem C cycle research.

727 Our soil gas and porewater chemistry indicate that the measured differences in elemental
728 composition influence the C cycle and weathering reactions in our watershed and impart strong
729 spatial heterogeneity on CO₂ partitioning between gas and aqueous phase. High soil moisture and
730 neutral pH buffered by carbonate minerals at the midslopes drove CO₂ dissolution and imparted
731 an ARQ lower at the midslopes than the ridgetop. Differences in soil mineralogy controlled
732 further CO₂ dissolution through carbonate weathering reactions. While accounting for some of
733 the carbonate weathering, nitrification did not have a measurable effect on the soil CO₂ at Cole
734 Farm. We conclude that assessing soil and lithologic properties is key when measuring the soil C
735 cycle in a watershed. Furthermore, our results provide strong evidence that DIC can be a
736 significant component of the C cycle in humid, temperate watersheds. In our case, surface soil
737 CO₂ efflux would greatly underestimate soil respiration, confounding efforts to construct or
738 simulate the soil C cycle using traditional surface efflux measurements. Globally, these
739 carbonate system reactions have the capacity to alter the balance of C pools and fluxes in many
740 ecosystems, especially with shifting land use.

741

742 **Acknowledgments, Samples, and Data**

743 Financial Support was provided by National Science Foundation Grant EAR – 1331726
744 to SLB for SSHCZO and NIFA Predoctoral Fellowship 2020-67034-31716 to CH. This research
745 was conducted on a farm in Shaver's Creek watershed at the intersection of RT 305 and
746 Winchester Road and we acknowledge the support of the owner, H. Cole. Thanks to Benjamin
747 Dillner and Brosi Bradley for field assistance and Xin Gu, Alison Richards, and Perri Silverhart
748 for rock sampling and interpretation of regional geology and mineralogy. Porewaters and rocks
749 were analyzed at the Laboratory for Isotopes and Metals in the Environment at Pennsylvania

750 State University. Soil moisture time series, soil profile descriptions, and soil profile
751 geochemistry are available at czo.psu.edu. Soil porewater chemistry and soil pCO₂ and pO₂ will
752 be published as coordinated datasets in Pangaea (pangaea.de).

753

754 **References**

- 755 Amundson, R. (2001). The Carbon Budget in Soils. *Annual Review of Earth and Planetary*
756 *Sciences*, 29(1), 535–562. <https://doi.org/10.1146/annurev.earth.29.1.535>
- 757 Ahmad, W., Singh, B., Dalal, R. C., & Dijkstra, F. A. (2015). Carbon dynamics from carbonate
758 dissolution in Australian agricultural soils. *Soil Research*, 53(2), 144–153.
759 <https://doi.org/10.1071/sr14060>
- 760 Angert, A., Yakir, D., Rodeghiero, M., Preisler, Y., Davidson, E. A., & Weiner, T. (2015). Using
761 O₂ to study the relationships between soil CO₂ efflux and soil respiration. *Biogeosciences*,
762 12(7), 2089–2099. <https://doi.org/10.5194/bg-12-2089-2015>
- 763 Bargrizan, S., Smernik, R. J., & Mosley, L. M. (2020). Constraining the carbonate system in soils
764 via testing the internal consistency of pH, pCO₂ and alkalinity measurements. *Geochemical*
765 *Transactions*, 21(1), 4. <https://doi.org/10.1186/s12932-020-00069-5>
- 766 Batjes, N. (2016). Harmonized soil property values for broad-scale modelling (WISE30sec) with
767 estimates of global soil carbon stocks *Geoderma* 269, 61-68.
768 <https://dx.doi.org/10.1016/j.geoderma.2016.01.034>
- 769 Brantley, S.L., Lebedeva, M., & Bazilevskaya, E. (2014). *Treatise on Geochemistry (Second*
770 *Edition)*. 327–352. <https://doi.org/10.1016/B978-0-08-095975-7.01317-6>
- 771 Brantley, S.L., Holleran, M. E., Jin, L., & Bazilevskaya, E. (2013). Probing deep weathering in
772 the Shale Hills Critical Zone Observatory, Pennsylvania (USA): The hypothesis of nested
773 chemical reaction fronts in the subsurface. *Earth Surface Processes and Landforms*, 38(11),
774 1280–1298. <https://doi.org/10.1002/esp.3415>
- 775 Butman, D., & Raymond, P. A. (2011). Significant efflux of carbon dioxide from streams and
776 rivers in the United States. *Nature Geoscience*, 4(12), 839. <https://doi.org/10.1038/ngeo1294>
- 777 Cerling, T. E. (1984). The stable isotopic composition of modern soil carbonate and its
778 relationship to climate. *Earth and Planetary Science Letters*, 71(2), 229–240.
779 [https://doi.org/10.1016/0012-821x\(84\)90089-x](https://doi.org/10.1016/0012-821x(84)90089-x)
- 780 Chadwick, O. A., Kelly, E. F., Merritts, D. M., & Amundson, R. G. (1994). Carbon dioxide
781 consumption during soil development. *Biogeochemistry*, 24(3), 115–127. [https://doi.org/10.1007/](https://doi.org/10.1007/bf00003268)
782 [bf00003268](https://doi.org/10.1007/bf00003268)
- 783 Cueva, A., Volkmann, T. H. M., Haren, J. van, Troch, P. A., & Meredith, L. K. (2019).
784 Reconciling Negative Soil CO₂ Fluxes: Insights from a Large-Scale Experimental Hillslope. *Soil*
785 *Systems*, 3(1), 10. <https://doi.org/10.3390/soilsystems3010010>
- 786 Doane, T. A., & Horwath, W. R. (2003). Spectrophotometric determination of nitrate with a
787 single reagent. *Analytical Letters*, 36(12), 2713–2722. <https://doi.org/10.1081/AL-120024647>

- 788 Gandois, L., Perrin, A.-S., & Probst, A. (2011). Impact of nitrogenous fertiliser-induced proton
789 release on cultivated soils with contrasting carbonate contents: A column experiment.
790 *Geochimica et Cosmochimica Acta*, 75(5), 1185–1198. <https://doi.org/10.1016/j.gca.2010.11.025>
- 791 Gu, X., Mavko, G., Ma, L., Oakley, D., Accardo, N., Carr, B. J., et al. (2020). Seismic refraction
792 tracks porosity generation and possible CO₂ production at depth under a headwater catchment.
793 *Proceedings of the National Academy of Sciences*, 117(32), 18991–18997.
794 <https://doi.org/10.1073/pnas.2003451117>
- 795 Hamerlynck, E. P., Scott, R. L., Sánchez-Cañete, E. P., & Barron-Gafford, G. A. (2013).
796 Nocturnal soil CO₂ uptake and its relationship to subsurface soil and ecosystem carbon fluxes in
797 a Chihuahuan Desert shrubland. *Journal of Geophysical Research: Biogeosciences*, 118(4),
798 1593–1603. <https://doi.org/10.1002/2013jg002495>
- 799 Hamilton, S. K., Kurzman, A. L., Arango, C., Jin, L., & Robertson, G. P. (2007). Evidence for
800 carbon sequestration by agricultural liming. *Global Biogeochemical Cycles*, 21(2).
801 <https://doi.org/10.1029/2006gb002738>
- 802 Hasenmueller, E., Jin, L., Stinchcomb, G., Lin, H., Brantley, S., Kaye, J. (2015). Topographic
803 controls on the depth distribution of soil CO₂ in a small temperate watershed. *Applied*
804 *Geochemistry*. 63, 58-69. <https://dx.doi.org/10.1016/j.apgeochem.2015.07.005>
- 805 Hodges, C., Kim, H., Brantley, S. L., & Kaye, J. (2019). Soil CO₂ and O₂ Concentrations
806 Illuminate the Relative Importance of Weathering and Respiration to Seasonal Soil Gas
807 Fluctuations. *Soil Science Society of America Journal*. <https://doi.org/10.2136/sssaj2019.02.0049>
- 808 Jin, L., Ogrinc, N., Yesavage, T., Hasenmueller, E. A., Ma, L., Sullivan, P. L., et al. (2014). The
809 CO₂ consumption potential during gray shale weathering: Insights from the evolution of carbon
810 isotopes in the Susquehanna Shale Hills critical zone observatory. *Geochimica et Cosmochimica*
811 *Acta*, 142, 260–280. <https://doi.org/10.1016/j.gca.2014.07.006>
- 812 Kim, H., Stinchcomb, G., & Brantley, S. L. (2017). Feedbacks among O₂ and CO₂ in deep soil
813 gas, oxidation of ferrous minerals, and fractures: A hypothesis for steady-state regolith thickness.
814 *Earth and Planetary Science Letters*, 460, 29–40. <https://doi.org/10.1016/j.epsl.2016.12.003>
- 815 Kim, J. H., Jobbágy, E. G., Richter, D. D., Trumbore, S. E. & Jackson, R. B. (2020). Agricultural
816 acceleration of soil carbonate weathering. *Global Change Biology*. 26, 5988–6002.
817 [10.1111/gcb.15207](https://doi.org/10.1111/gcb.15207)
- 818 Kindler, R., Siemens, J., Kaiser, K., Walmsley, D. C., Berhoffer, C., Buchmann, N., Cellar, P.,
819 Eugster, W., Gliexner, G., Grunwald, T., Heim, A., Ibrom, A., Jones, S. K., Jones, M., Klumpp,
820 K., Kutsch, W., Larsen, K. S., Lehuger, S., Loubett, B., ... Kaupenjohann, M. (2011). Dissolved
821 carbon leaching from soil is a crucial component of the net ecosystem carbon balance. *Global*
822 *Change Biology*, 17(2), 1167–1185. <https://doi.org/10.1111/j.1365-2486.2010.02282.x>
- 823 Kowalski, A. S., Serrano-Ortiz, P., Janssens, I. A., Sánchez-Moral, S., Cuezva, S., Domingo, F.,
824 Were, A., & Alados-Arboledas, L. (2008). Can flux tower research neglect geochemical CO₂
825 exchange? *Agricultural and Forest Meteorology*, 148(6–7), 1045–1054.
826 <https://doi.org/10.1016/j.agrformet.2008.02.004>
- 827 Li, L., Bao, C., Sullivan, P. L., Brantley, S., Shi, Y., & Duffy, C. (2017). Understanding
828 watershed hydrogeochemistry: 2. Synchronized hydrological and geochemical processes drive

- 829 stream chemostatic behavior. *Water Resources Research*, 53(3), 2346–2367.
830 <https://doi.org/10.1002/2016wr018935>
- 831 Li, L., DiBiase, R. A., Vecchio, J. D., Marcon, V., Hoagland, B., Xiao, D., Wayman, C., Tang, Q.,
832 He, Y., Silverhart, P., Szink, I., Forsythe, B., Williams, J. Z., Shapich, D., Mount, G. J., Kaye, J.,
833 Guo, L., Lin, H., Eissenstat, D., ... Brantley, S. L. (2018). The Effect of Lithology and
834 Agriculture at the Susquehanna Shale Hills Critical Zone Observatory. *Vadose Zone Journal*,
835 17(1), 0. <https://doi.org/10.2136/vzj2018.03.0063>
- 836 Liu, J., Fa, K., Zhang, Y., Wu, B., Qin, S., & Jia, X. (2015). Abiotic CO₂ uptake from the
837 atmosphere by semiarid desert soil and its partitioning into soil phases. *Geophysical Research*
838 *Letters*, 42(14), 5779–5785. <https://doi.org/10.1002/2015gl064689>
- 839 Liu, T., Wang, L., Feng, X., Zhang, J., Ma, T., Wang, X., & Liu, Z. (2018a). Comparing soil
840 carbon loss through respiration and leaching under extreme precipitation events in arid and
841 semiarid grasslands. *Biogeosciences*, 15(5), 1627–1641. [https://doi.org/10.5194/bg-15-1627-](https://doi.org/10.5194/bg-15-1627-2018)
842 2018
- 843 Liu, T., Wang, L., Feng, X., Zhang, J., Ma, T., Wang, X., & Liu, Z. (2018b). Comparing soil
844 carbon loss through respiration and leaching under extreme precipitation events in arid and
845 semiarid grasslands. *Biogeosciences*, 15(5), 1627–1641. [https://doi.org/10.5194/bg-15-1627-](https://doi.org/10.5194/bg-15-1627-2018)
846 2018
- 847 Lloyd, J., & Taylor, J. (1994). On the Temperature Dependence of Soil Respiration. *Functional*
848 *Ecology*, 8(3), 315–323. doi:10.2307/2389824
- 849 Mikhailova, E. A., & Post, C. J. (2006). Effects of Land Use on Soil Inorganic Carbon Stocks in
850 the Russian Chernozem. *Journal of Environmental Quality*, 35(4), 1384–1388.
851 <https://doi.org/10.2134/jeq2005.0151>
- 852 NADP (National Atmospheric Deposition Program). (2018). Leading Ridge (PA42) site, annual
853 precipitation-weighted means [Data set]. Retrieved from <http://nadp.sws.uiuc.edu/data/NTN/>
- 854 Nychka, D., R. Furrer, J. Paige, and S. Sain. 2017. *Fields: Tools for spatial data*. University
855 Corporation for Atmospheric Research, Boulder, CO. doi:10.5065/D6W957CT
- 856 Oleson, K. W., Lawrence, D. M., Gordon, B., Flanner, M. G., Kluzek, E., Peter, J., ... & Heald,
857 C. L. (2010). Technical description of version 4.0 of the Community Land Model (CLM).
- 858 Olshansky, Y., Knowles, J. F., Barron–Gafford, G. A., Rasmussen, C., Abramson, N., &
859 Chorover, J. (2019). Soil Fluid Biogeochemical Response to Climatic Events. *Journal of*
860 *Geophysical Research: Biogeosciences*. <https://doi.org/10.1029/2019jg005216>
- 861 Pacific, V. J., McGlynn, B. L., Riveros-Iregui, D. A., Welsch, D. L., & Epstein, H. E. (2010).
862 Landscape structure, groundwater dynamics, and soil water content influence soil respiration
863 across riparian-hillslope transitions in the Tenderfoot Creek Experimental Forest, Montana.
864 *Hydrological Processes*, 25(5), 811–827. <https://doi.org/10.1002/hyp.7870>
- 865 Perrin, A.-S., Probst, A., & Probst, J.-L. (2008). Impact of nitrogenous fertilizers on carbonate
866 dissolution in small agricultural catchments: Implications for weathering CO₂ uptake at regional
867 and global scales. *Geochimica et Cosmochimica Acta*, 72(13), 3105–3123.
868 <https://doi.org/10.1016/j.gca.2008.04.011>

- 869 R Core Team. 2018. R: A language and environment for statistical computing. R Foundation for
870 Statistical Computing, Vienna, Austria.
- 871 Raich, J. W., & Schlesinger, W. H. (1992). The global carbon dioxide flux in soil respiration and
872 its relationship to vegetation and climate. *Tellus B: Chemical and Physical Meteorology*, 44(2),
873 81–99. <https://doi.org/10.3402/tellusb.v44i2.15428>
- 874 Raza S., N. Miao, P. Wang, X. Ju, Z. Chen, J. Zhou, Y. Kuzyakov. (2020). Dramatic loss of
875 inorganic carbon by nitrogen-induced soil acidification in Chinese croplands. *Global Change*
876 *Biology*. 26, 3738–3751. 10.1111/gcb.15101
- 877 Rey, A. (2015). Mind the gap: Non-biological processes contributing to soil CO₂ efflux. *Global*
878 *Change Biology*, 21(5), 1752–1761. <https://doi.org/10.1111/gcb.12821>
- 879 Sánchez-Cañete, E. P., Barron-Gafford, G. A., & Chorover, J. (2018). A considerable fraction of
880 soil-respired CO₂ is not emitted directly to the atmosphere. *Scientific Reports*, 8(1), 13518.
881 <https://doi.org/10.1038/s41598-018-29803-x>
- 882 Sanderman, J. (2012). Can management induced changes in the carbonate system drive soil
883 carbon sequestration? A review with particular focus on Australia. *Agriculture, Ecosystems &*
884 *Environment*, 155, 70–77. <https://doi.org/10.1016/j.agee.2012.04.015>
- 885 Schindlbacher, A., Beck, K., Holzheu, S., & Borcken, W. (2019). Inorganic Carbon Leaching
886 From a Warmed and Irrigated Carbonate Forest Soil. *Frontiers in Forests and Global Change*, 2,
887 40. <https://doi.org/10.3389/ffgc.2019.00040>
- 888 Serrano-Ortiz, P., Roland, M., Sanchez-Moral, S., Janssens, I. A., Domingo, F., Godd eris, Y., &
889 Kowalski, A. S. (2010). Hidden, abiotic CO₂ flows and gaseous reservoirs in the terrestrial
890 carbon cycle: Review and perspectives. *Agricultural and Forest Meteorology*, 150(3), 321–329.
891 <https://doi.org/10.1016/j.agrformet.2010.01.002>
- 892 Shi, Y., Eissenstat, D. M., He, Y., & Davis, K. J. (2018). Using a spatially-distributed hydrologic
893 biogeochemistry model with a nitrogen transport module to study the spatial variation of carbon
894 processes in a Critical Zone Observatory. *Ecological Modelling*, 380, 8–21.
895 <https://doi.org/10.1016/j.ecolmodel.2018.04.007>
- 896 Silverhart, P. (2019). *Land use versus climate controls on hillslope erosion at a farmed*
897 *headwater catchment in central Pennsylvania* (Unpublished Master’s Thesis). Pennsylvania
898 State University, University Park, PA.
- 899 Sims, G. K., Ellsworth, T. R., & Mulvaney, R. L. (1995). Microscale determination of inorganic
900 nitrogen in water and soil extracts. *Communications in Soil Science and Plant Analysis*, 26(1–2),
901 303–316. <https://doi.org/10.1080/00103629509369298>
- 902 Stumm, W., & Morgan, J. J. (1996). *Aquatic Chemistry*. 477.
- 903 Thenkabail, P., Knox, J., Ozdogan, M., Gumma, M., Congalton, R., Wu, Z., Milesi, C., Finkral,
904 A., Marshall, M., Mariotto, I., You, S., Giri, C., Nagler, P. (2016). NASA Making Earth System
905 Data Records for Use in Research Environments (MEaSUREs) Global Food Security Support
906 Analysis Data (GFSAD) Crop Dominance 2010 Global 1 km V001 [Data set]. NASA EOSDIS
907 Land Processes DAAC. Accessed 2020-01-23 from
908 <https://doi.org/10.5067/MEaSUREs/GFSAD/GFSAD1KCD.001>

- 909 Thornton, P. E., Law, B. E., Gholz, H. L., Clark, K. L., Falge, E., Ellsworth, D. S., Goldstein, A.
910 H., Monson, R. K., Hollinger, D., Falk, M., Chen, J., & Sparks, J. P. (2002). Modeling and
911 measuring the effects of disturbance history and climate on carbon and water budgets in
912 evergreen needleleaf forests. *Agricultural and Forest Meteorology*, *113*(1), 185–222.
- 913 Tsutsui, H., Fujiwara, T., Inoue, D., Ito, R., Matsukawa, K., & Funamizu, N. (2015). Relationship
914 between respiratory quotient, nitrification, and nitrous oxide emissions in a forced aerated
915 composting process. *Waste Management*, *42*, 10–16.
916 <https://doi.org/10.1016/j.wasman.2015.02.038>
- 917 West, T. O., & McBride, A. C. (2005). The contribution of agricultural lime to carbon dioxide
918 emissions in the United States: dissolution, transport, and net emissions. *Agriculture, Ecosystems*
919 *& Environment*, *108*(2), 145–154. <https://doi.org/10.1016/j.agee.2005.01.002>
- 920 Wu, L., Wood, Y., Jiang, P., Li, L., Pan, G., Lu, J., et al. (2008). Carbon Sequestration and
921 Dynamics of Two Irrigated Agricultural Soils in California. *Soil Science Society of America*
922 *Journal*, *72*(3), 808–814. <https://doi.org/10.2136/sssaj2007.0074>
- 923 Zamanian, K., Pustovoytov, K., & Kuzyakov, Y. (2016). Pedogenic carbonates: Forms and
924 formation processes. *Earth-Science Reviews*, *157*, 1–17.
925 <https://doi.org/10.1016/j.earscirev.2016.03.003>
- 926 Zamanian, K., Zarebanadkouki, M., & Kuzyakov, Y. (2018). Nitrogen fertilization raises CO₂
927 efflux from inorganic carbon: A global assessment. *Global Change Biology*, *24*(7), 2810–2817.
928 <https://doi.org/10.1111/gcb.14148>
- 929 Zamanian, K., Zhou, J., & Kuzyakov, Y. (2021). Soil carbonates: The unaccounted, irrecoverable
930 carbon source. *Geoderma*, *384*, 114817. <https://doi.org/10.1016/j.geoderma.2020.114817>